Heliyon 10 (2024) e38943

Contents lists available at ScienceDirect

Heliyon

journal homepage: www.cell.com/heliyon

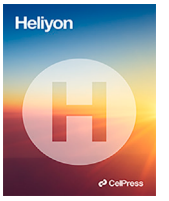

Research article

Experimental validation of a novel hybrid Equilibrium Slime Mould Optimization for solar photovoltaic system

Djallal Eddine Zabia [a], Hamza Afghoul [b], Okba Kraa [c], Yassine Himeur [d,*], Haitham S. Ramadan [e,f], Istemihan Genc [g], Abdoulkader I. Idriss [h], Sami Miniaoui [d], Shadi Atalla [d], Wathiq Mansoor [d]

[a] *Laboratory of Identification, Command, Control and Communication (LI3CUB), University of Biskra, Algeria*
[b] *LAS Laboratory, Faculty of Technology, Ferhat Abbas Setif-1 University, Algeria*
[c] *Laboratory of Energy System Modeling Electrical Engineering (LMSE), Algeria*
[d] *College of Engineering and Information Technology, University of Dubai, Dubai, United Arab Emirates*
[e] *Electrical Power and Machines Department, Faculty of Engineering, Zagazig University, Egypt*
[f] *ISTHY, Institut International sur le Stockage de l'Hydrogene, 90400 Meroux-Moval, France*
[g] *Department of Electrical Engineering, Istanbul Technical University, Istanbul 34469, Turkey*
[h] *Electrical and Energy Department, Faculty of Engineering, University of Djibouti, Street Djanaleh, 1904, Djibouti*

ARTICLE INFO

Keywords:
Renewable energy
Complex partial shading condition
Equilibrium Slime Mould optimization algorithm
Maximum power point tracking
Photovoltaic system

ABSTRACT

Maximizing Power Point Tracking (MPPT) is an essential technique in photovoltaic (PV) systems that guarantees the highest potential conversion of sunlight energy under any irradiance changes. Efficient and reliable MPPT technique is a challenge faced by researchers due to factors such as fluctuations in irradiance and the presence of partial shading. This paper introduced a novel hybrid Equilibrium Slime Mould Optimization (ESMO) MPPT-based algorithm combining the advantages of two recent algorithms, Slime Mould Optimization (SMO) and Equilibrium Optimizer (EO). The ESMO algorithm is compared with highly efficient MPPT-based techniques such as SMO, EO, Particle Swarm Optimization (PSO), Grey Wolf Optimization (GWO), and Whale Optimization Algorithm (WOA), both under a Simulink environment and a real-time experimental laboratory setup using a Dspace1104 controller and PV emulator. The comparison focuses on performance under several irradiance cases, including instant irradiance change, partial shading, complex partial shading, and dynamic partial shading. The key advantage of ESMO is the fact that it has a single tunable parameter, which makes implementation much easier and, at the same time, reduces the computational resources that are required by the control system. Extensive testing proves the superiority of ESMO over all other techniques, the average efficiency of which is 99.98% under all conditions. Additionally, ESMO provides fast average tracking times of 244 ms under simulation experiments and 200 ms for real-time experiments. These results show that ESMO can be very important for future implementation in large-scale solar PV systems.

* Corresponding author.
E-mail addresses: djallaleddine.zabia@univ-biskra.dz (D.E. Zabia), yhimeur@ud.ac.ae (Y. Himeur).

https://doi.org/10.1016/j.heliyon.2024.e38943
Received 16 September 2023; Received in revised form 22 September 2024; Accepted 2 October 2024

Available online 9 October 2024

Nomenclature

α	Ideality factor	q	Elementary charge
μ_{id}	Inductor current ripple	R_s	Series resistance
μ_{vd}	Load voltage ripple	$R_{s,eq}$	Equivalent series resistance
C_{input}	Input capacitance	$R_{sh,eq}$	Equivalent shunt resistance
C_{output}	Output capacitance	R_{sh}	Shunt resistance
D_{cycle}	Duty cycle	T	Temperature
f_{sw}	Switching frequency	T_{Sc}	Standard test condition temperature
G	Irradiance	V_{input}	Input voltage
G_{Sc}	Standard test condition irradiance	V_{mpp}	Voltage at maximum power point
I_d	Diode current	V_{oc}	Open-circuit voltage
I_{mpp}	Current at maximum power point	V_{output}	Output voltage
I_{ph}	Photocurrent	V_T	Thermal voltage
I_{pv}	Photocurrent of a single cell	DCL	Duty Cycle
I_{sat}	Dark saturation current	DCUT	Duty Cycle Update Timer
I_{sc}	Short-circuit current	DPSC	Dynamic Partial Shading Condition
K	Temperature coefficient of photocurrent	EO	Equilibrium Optimizer
k	Boltzmann constant	ESMO	Equilibrium Slime Mould Optimization
L	Inductance	GMPP	Global Maximum Power Point
N_p	Number of cells in parallel	I	Total current
N_s	Number of cells in series	P-V curve	Power-Voltage curve
N_{cs}	Number of cells in a module	PSC	Partial Shading Condition
P_{max}	Maximum power	PV	Photovoltaic

1. Introduction

Renewable energy sources, particularly solar energy (SE), are regarded as one of the foremost mechanisms humanity is looking to depend on during this advanced environmental pollution and climate change [1,2]. It is generated by the sun through thermonuclear fusion reactions, and solar panels transform it into electricity for human usage. Photovoltaic (PV) systems play a crucial role in harnessing SE. Still, their efficiency can be impacted by diverse, dynamic environmental elements, such as fast irradiance changes (FIC) and partial shading conditions (PSC) [3,4]. Such panels are created using advanced semiconductor technologies, which have become integral to electronic manufacturing in recent decades [5]. Solar panels exhibit a unique Power-Voltage curve that showcases the characteristics of the cell [6]. Despite the many benefits of SE, such as the fact that it is a clean, permanent renewable energy source with low maintenance costs, it still has drawbacks in power losses and manufacturing and installation costs [7]. This prompted researchers in renewable energies to dedicate considerable time and resources to enhance the solar cell's efficiency in manufacturing and energy production. One of these is the field of research into determining a cell's maximum possible power, mathematically represented by the maximum power point (MPP) on the PV curve.

Utilizing the power electronic converter, a pivotal component within the PV system, tracking and maintaining the reference voltage and current became necessary, guaranteeing the highest recorded power at the output [8]. A single peak is created in the PV curve in the case of uniform Irradiation. Still, the hotspots phenomenon is created by clouds, leaves, or any shaded object, resulting in current unmatching between modules. A bypass diode compensates for this problem, resulting in several peaks in the PV curve [9]. Researchers have been exploring advanced optimization techniques to overcome these challenges and improve the performance of PV systems. One encouraging approach involves the integration of modern Maximum Power Point Tracking (MPPT) techniques, EO, and Slime Mould Optimization (SMO) under the name Equilibrium Slime Mould Optimization (ESMO). The concept of ESMO aims to leverage the strengths of both EO and SMO to amplify the overall efficiency of PV systems in dynamic environments. By integrating the Equilibrium Pool tool of EO into one of the SMO equations, ESMO facilitates faster convergence to the optimum solution and helps overcome the issue of local optimum trapping [10].

1.1. Literature review

According to the existing literature, MPPT is a crucial aspect of PV systems [11]. Researchers have invested considerable effort into studying and implementing various mathematical techniques to calculate and identify the MPP on the PV curve. Conventional algorithms like Perturb & Observe (P&O), Incremental Conductance (INC), and Hill Climbing (HC) have been proposed as techniques to track the MPP. However, these methods are limited to uniform irradiation conditions with a single peak on the PV curve, and they exhibit oscillation at the MPP [12,13]. In scenarios involving PSC and the formation of multiple peaks, conventional techniques can become trapped at local points, leading to a substantial loss of system power [14,15]. Researchers have explored solutions using soft computing and intelligent techniques to address this limitation. Methods such as Neural Networks MPPT algorithm [16] and Fuzzy Logic-based MPPT [17] Have been harnessed to determine the MPP. However, these approaches often require significant

Table 1
Summarized overview of the recent technique.

Authors	Technique	Summary
Shiau et al. [25]	Fuzzy-Logic-Based	Standard MPPT technique based on fuzzy logic with a variety of inputs where the sum of the arctangent of conductance and the arctangent of INC with the lowest average reaching the time of 0.053 s.
Husain et al. [26]	Spider monkey	Spider Monkey Optimization technique, which uses the social structure principle of fission-fusion of spider monkeys, reduced steady-state, transient error, and settling time to 3 ms, compared to the conventional PSO and P&O methods.
Aljafari et al. [27]	Butterfly optimization	Hybrid Opposition-based reinforcement learning-butterfly optimization algorithm (OBR-BOA) record the highest average efficiencies with three different PV configurations under three different PSC scenarios with 99.8%,99.72%, and 98.50%, beaten the basic BOA, WOA, GWO, and PSO.
Ghazi et al. [28]	Circle Search Algorithm	A Circle Search Algorithm-Based Super Twisting Sliding Mode Control (CSA-STSMC) achieves an improvement between 0.1% and 0.5% of tracking the MPP under non-standard conditions, with the lowest ITAE of 0.89 of the regulation closed-loop compared to the other used methods CSA-PI, GWO-STSMC and InC-PI.
Xia et al. [29]	Ant-Fuzzy Optimization	Hardware dSPACE real-time test of the hybrid Ant colony and Fuzzy logic technique (AFO) reaches 98.7% accuracy with 0.9 s tracking time compared to basic ACO, FL and PSO under PSC.
Yuan et al. [30]	Hermite Interpolation Optimization	Hermite interpolation optimization (HPO) uses a fixed step on INC algorithm to improve tracking capability under PSC; it was able to achieve an average efficiency of 99.84% in 4 different scenarios against the conventional technique P&O and INC.
Qi et al. [31]	hybrid Cuckoo-Bee Colony	A hybrid of the well-known Cuckoo Search Algorithm and Artificial Bee Colony algorithm (CSA-ABC) reaches a surplus efficiency from 7-80%, outperforming the basic CSA, ABC, and PSO under different PSC cases.
Kumar et al. [32]	Adaptive Flower Pollination Algorithm	An improved version of the basic flower pollination algorithm (AFPA) produced energy up to 2.5% compared to FPA and reduced the tracking time by over 40% compared to PSO under uniform case, weak PSC, moderate PSC, and strong PSC
Yu et al. [33]	Quantum-behavior particle swarm optimization	Premature convergence issue of conventional QPSO was addressed by modifying the contraction–expansion coefficient. Improved QPSO reaches efficacies of 99.91% and 99.47% of single peak and multiple peaks, respectively, compared to QPSO, FA, and PSO under experimental results.
Ghazi et al. [34]	Dandelion optimizer	DO combined with Deep Reinforcement Learning (DRL) was used to regulate the voltage reference of MPPT. DO-DRL scores a high efficiency of 85.90% and 95% under summer day and winter day, respectively, compared to the other methods PSO-DRL, PSO-PI, DO-PI, and InC-PI.
Ha et al. [35]	Artificial Location Selection Optimization	The proposed ALSO reaches near perfect 100% reference MPP voltage tracking efficiency with simulation and over 95% with experimental setup assisted with Chroma 62100H PV emulator under five districts PSC curves.
Naser et al. [36]	Coot optimizer	Improved coot optimizer algorithm (ICOA) uses a new way to handle changes in power demand with only one tuning parameter, reaching an average efficiency of 99.94% and tracking time of 0.58 s under different PSCs with a SEPIC converter.
Chao et al. [37]	Intelligent bat algorithm	Improved Intelligent Bat Algorithm (IIBA) adjusts its search patterns based on the slope of the power curve, which allows it to outperform the CIBA, IFA, and MGWOA. IIBA scores by far the lowest average tracking time of 0.04 s compared to the other methods.
Chao et al. [38]	Cat swarm optimization	Modified cat swarm optimization (MCSO) adjusts its search speed based on two factors: the slope of the power output curve and an inertia weight. MCSO records the fastest average tracking time of 0.36 s and maximum oscillation amplitude of 9 W compared to the conventional CSO and the other 3 MCSO variants under 6 GMPP peak cases.

computational resources and may necessitate prior knowledge of the PV cell model [18]. Furthermore, a two-stage MPPT controller employing an ANFIS estimator and an MRAC has also been used in the literature for PV systems [19]. This approach effectively addresses dynamic environments and surpasses the conventional methods in convergence speed and tracking efficiency, but it is still not applicable under PSC. To overcome these challenges, metaheuristic algorithms have emerged, which do not rely on prior knowledge of the model and directly engage with the system. These algorithms leverage exploration and exploitation mechanisms to identify and approach the Global Maximum Power Point (GMPP) based on their mathematical behavior [20]. Metaheuristic algorithms can be categorized into evolutionary-based, physical-based, social-based, and swarm-based algorithms [21]. Some of the notable techniques used for MPPT on the PV curve include Short-Distance Running Algorithm (SDRA), Dragonfly Optimization (DFO), Social Ski Driver (SSD), Quantum Grover Search Algorithm, Salp Swarm Algorithm (SSA), Horse Herd Optimization Algorithm (HOA), Bat Algorithm (BA), Marine Predator Algorithm (MPA), Bald Eagle Search Optimization (BES), Harmony Search (HS) [22], SMO [23], and EO [24].

The presented overview in Table 1 summarizes recent techniques in the literature related to MPPT in PV systems. These metaheuristic algorithms hold promise for effectively tracking the MPP on the PV curve, offering potential solutions to the challenges posed by PSC scenarios.

1.2. Motivation behind the work

In recent years, utilizing metaheuristic algorithms has experienced notable expansion, addressing diverse system problems and receiving positive feedback from researchers [39]. These techniques have been particularly leveraged for identifying the MPP on the PV curve due to their simplicity of implementation and low computational resource requirements [40,41]. Efficiency, reaching time, convergence time, and the number of iterations are key factors used to compare the performance of different MPP tracking techniques.

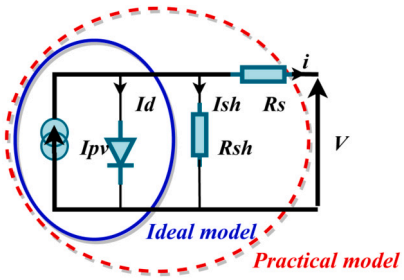

Fig. 1. Practical 1M5P PV model.

CPS scenarios, characterized by the formation of multiple nearby clusters of peaks, pose challenges for some algorithms in identifying the MPP, searching for the optimal solution more intricate [42,43]. However, the Grey Wolf Optimization (GWO) algorithm has demonstrated superiority over other techniques in terms of efficiency, requiring a smaller number of iterations and faster convergence to the MPP [44]. Meanwhile, when navigating the search space, these algorithms face the issue of the optimal solution changing over time. In response, researchers have undertaken the re-implementation of arithmetic operations and the re-initialization of solutions within the algorithms, aimed at inducing deviation from the preceding optimal solution [45]. The behavior of the algorithms is influenced by intelligent random solution selection and updating based on their mathematical principles. However, randomness can cause large fluctuations after obtaining the optimal solution, particularly noticeable in the Particle Swarm Optimization (PSO) algorithm [46]. The study [47] compares the proposed improved MPPT technique combining PSO with P&O and a predefined search space optimized through Fuzzy Fokker Planck solutions with conventional PI, fuzzy, and PSO controllers, demonstrating superior algorithm convergence, reduced oscillation around the MPP, and faster response times. The hardware and simulation results show the method's robustness in handling conditions such as partial shading, dust, and GHG concentration, achieving a maximum efficiency of 99.23%. However, the reliance on fuzzy logic tuning adds complexity to the algorithm, which might increase computational overhead in real-time applications. Researchers have introduced expressions related to the iteration number to mitigate these issues and organize the search phase into exploration and exploitation stages, thereby balancing both phases. For instance, the SMO algorithm employs three sub-equations for process control during the exploration and exploitation phases. However, formulating these sub-equations can slow down the search process [48], warranting further enhancements and streamlining for optimal solution convergence. One of the attempts is in Xiao et al. paper [49] with a hybrid slime mold golden sine algorithm (SMGSA) to help enhance the performance of the SMA by modifying the third equation with the golden sine concept. However, the algorithm still needs more than one parameter for tuning. In this context, this paper puts forth an innovative approach, a hybrid algorithm with high efficiency and rapid convergence to the optimal global solution with just one tunable parameter, addressing the mentioned issues and advancing the field of MPP tracking in PV systems. The proposed approach offers promising potential for efficient and effective MPP tracking, particularly in challenging scenarios like CPSC.

To address the limitations of previous MPPT techniques concerning efficiency, tracking speed, convergence to the MPP, and the number of iterations required in various PV system scenarios, a new approach is proposed based on the hybridization of two modern algorithms, SMO and EO. The primary contributions of this research are as follows:

- Study of the PV system using the novel hybrid ESMO approach, applied to three cases: FIC, partial shading, and complex CPSC.
- Introduction of the equilibrium pool concept to address the slow convergence issue in the SMO algorithm, resulting in a hybrid technique that efficiently and rapidly identifies the MPP with just one tunable parameter.
- Enhance efficiency and reliability through MPP identification in the PV as mentioned earlier system cases using the ESMO algorithm and comparison with various other techniques, including SMO, EO, GWO, WOA, and PSO.
- Implementation of laboratory experiments to verify the algorithm's strength under two conditions: Partial shading and Dynamic partial shading conditions.

Subsequent sections of the study are structured as follows: Section 2 delves into PV system modeling under uniform and PSC. In Section 3, the Hybrid proposed MPPT technique is introduced. Section 4 showcases and examines the research findings. Finally, Section 5 summarizes the research conclusions and perspectives.

2. PV system modeling under uniform and PSC

A PV cell is a direct power source, converting sunlight into electrical power [50]. Several mathematical models can represent it, including the single diode model depicted as the blue circle in Fig. 1. This model is regarded as a perfect portrayal of the electrical performance of the PV cell. The output current is determined using Equation (1) and Equation (2), which express it as the sum of the diode current. However, the single diode model exhibits certain weaknesses when environmental conditions change, particularly in low-voltage scenarios [51]. To address this, the practical model incorporates resistors R_s and R_{sh} into the circuit [52]. It is represented by the red dashed circle in Fig. 1, and it is mathematically expressed by Equation (3).

$$I_{pv} = I_{ph} - I_d \tag{1}$$

Table 2
PV array parameters.

Description	Values
P_{max}	316 W
V_{mpp}	39.5 W
I_{mpp}	8 A
V_{oc}	51.5 V
I_{sc}	8.5 A
K_V Temp-coefficient of Voc (%/deg.C)	-0.37
K_I Temp-coefficient of Isc (%/deg.C)	0.04
α	1.1612
N_{cs} (Number of cells in a module)	72

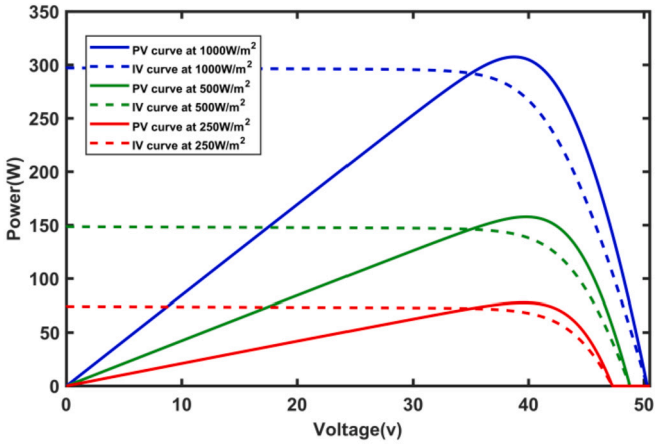

Fig. 2. The uniformed PV curve during the uniform case.

$$I_{pv} = I_{ph} - I_{sat}\left[e^{\frac{V}{\alpha \cdot V_T}} - 1\right] \tag{2}$$

$$I_{pv} = I_{ph} - I_{sat}\left[e^{\frac{V+IR_s}{\alpha \cdot V_T}} - 1\right] - \frac{V + IR_s}{R_{sh}} \tag{3}$$

$$V_T = \frac{N_s kT}{q} \tag{4}$$

Several PV cells are connected in both parallel and series configurations to form a PV panel, facilitating increased power production at the output [53]. The mathematical relationship expressing the arrangement of Ns cells in series and Np cells in parallel is presented in Equation (5).

$$I = I_{ph}N_p - N_p I_{sat}\left[e^{\frac{V+IR_{s.eq}}{N_{cs}\alpha \cdot V_T}} - 1\right] - \frac{V + IR_{s.eq}}{R_{sh.eq}} \tag{5}$$

The photoelectric current varies directly with the irradiance and exhibits an inverse relationship with the surrounding temperature. This relationship is mathematically described in Equation (6).

$$I_{pv} = (I_{pvSc} + K(T - T_{Sc})) \times \frac{G}{G_{Sc}} \tag{6}$$

Table 2 contains the electrical characteristics of the Sunpreme SNPM-GX-315 PV array used in this study. Fig. 2 shows the decrease in irradiance on the array leads to the formation of a uniform PV curve with a single power peak.

As shown in Fig. 3, when clouds or tree leaves cast shade on a portion of the PV array, the current in the shaded cells decreases, while the current in the uncovered cells remains unchanged. This phenomenon triggers the “hot spot” effect, leading to overheating in the array [54]. To address this issue, crosswire-connected bypass diodes are utilized to dissipate the self-heating caused by mismatched currents [55,56]. Consequently, multiple peaks appear along the PV curve, as illustrated in Fig. 4, showing a non-uniform PV curve with multiple local maximum power peaks (LMPP) and one global maximum power peak. Multiple peaks on the PV curve pose a challenge for most conventional algorithms when seeking the MPP, causing them to become trapped at the LMPP and hindering their ability to reach the GMPP [57,58]. In such cases, using metaheuristic algorithms becomes necessary to navigate the search space, represented by the PV curve, and obtain multiple values that align with the peak achievable power level.

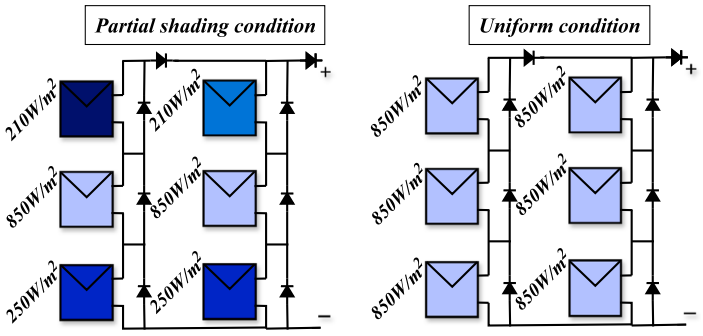

Fig. 3. PV array configurations with bypass diode during UC and PSC.

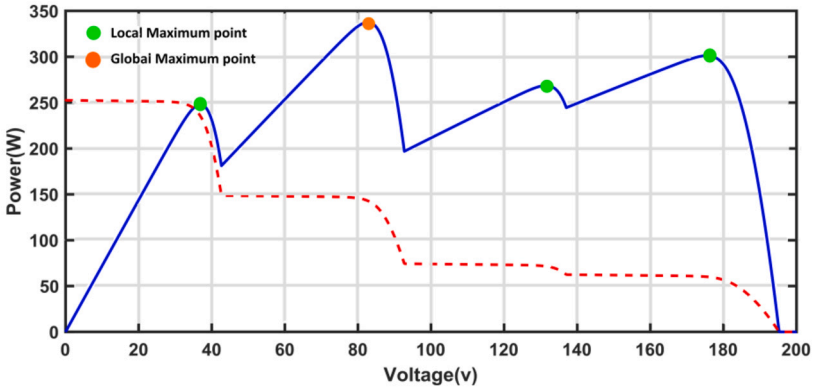

Fig. 4. The non-uniformed PV curve during the partial shading condition.

The DC-DC voltage boost converter regulates the PV voltage following the reference voltage corresponding to the MPP [59]. This control is achieved by manipulating the Duty Cycle (DCL), which spans from 0 to 1. Equation (7) details the formulas governing the boost converter.

$$\begin{cases} V_{output} = \frac{V_{input}}{1-D_{cycle}} \\ D_{cycle} = \frac{t_{on}}{t_{sw}} \\ C_{input} = \frac{\mu i_d}{8\mu i_d f_{sw}} \\ C_{output} = \frac{i_0 D_{cycle}}{8\mu v_d f_{sw}} \\ L = \frac{V_{pv} D_{cycle}}{2\mu i_d f_{sw}} \end{cases} \tag{7}$$

V_{input} and V_{output} represent the input and output voltage related to the boost converter, respectively. In contrast, C_{input} and C_{output} denote the input and output capacitances, respectively. Additionally, L corresponds to the required inductance. The inductor ripples current and the load ripple voltage are denoted as μI_d and μv_d, respectively, and the switching frequency is represented by f_{sw}.

3. The hybrid proposed MPPT

Metaheuristic algorithms provide a general search for the optimal solution within a given space, aligning with seeking the MPP on the PV curve. A new approach is proposed based on hybridizing two modern algorithms, SMO and EO. Under PSC, this hybrid algorithm effectively approaches the GMPP on the PV curve.

The two fundamental algorithms, SMA [23] and EO [24], are integrated to form the ESMO-based MPPT algorithm. The tracking mechanism is introduced as follows:

3.1. The Slime Mould Algorithm (SMA)

The slime mould “Physarum polycephalum” is an intelligent eukaryotic cell that utilizes a biological mechanism called bio-oscillation to guide cytoplasm diffusion through the veins formed by the group while searching for food. As the veins approach the

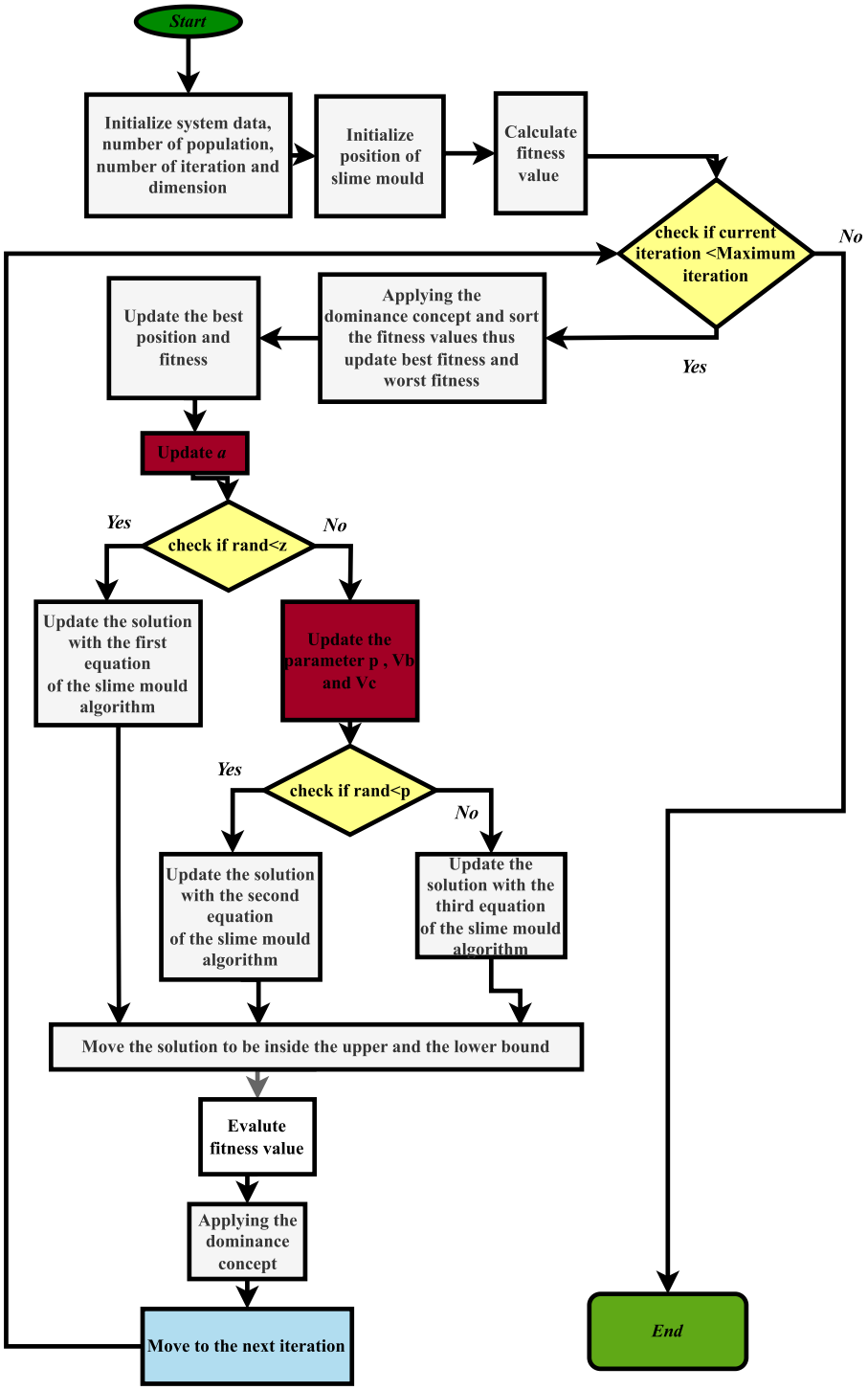

Fig. 5. The flowchart of SMA.

food source, the cytoplasm flow speed increases, resulting in thickening of the veins. This mechanism is employed to ascertain the optimal path for reaching the food source, guided by the ambient environmental odor. This mechanism was mathematically modeled, formulating a novel concept centered on weight modulation for governing positive and negative influence within the slime mould propagation wave [23]. The flow chart of the SMA is presented in Fig. 5.

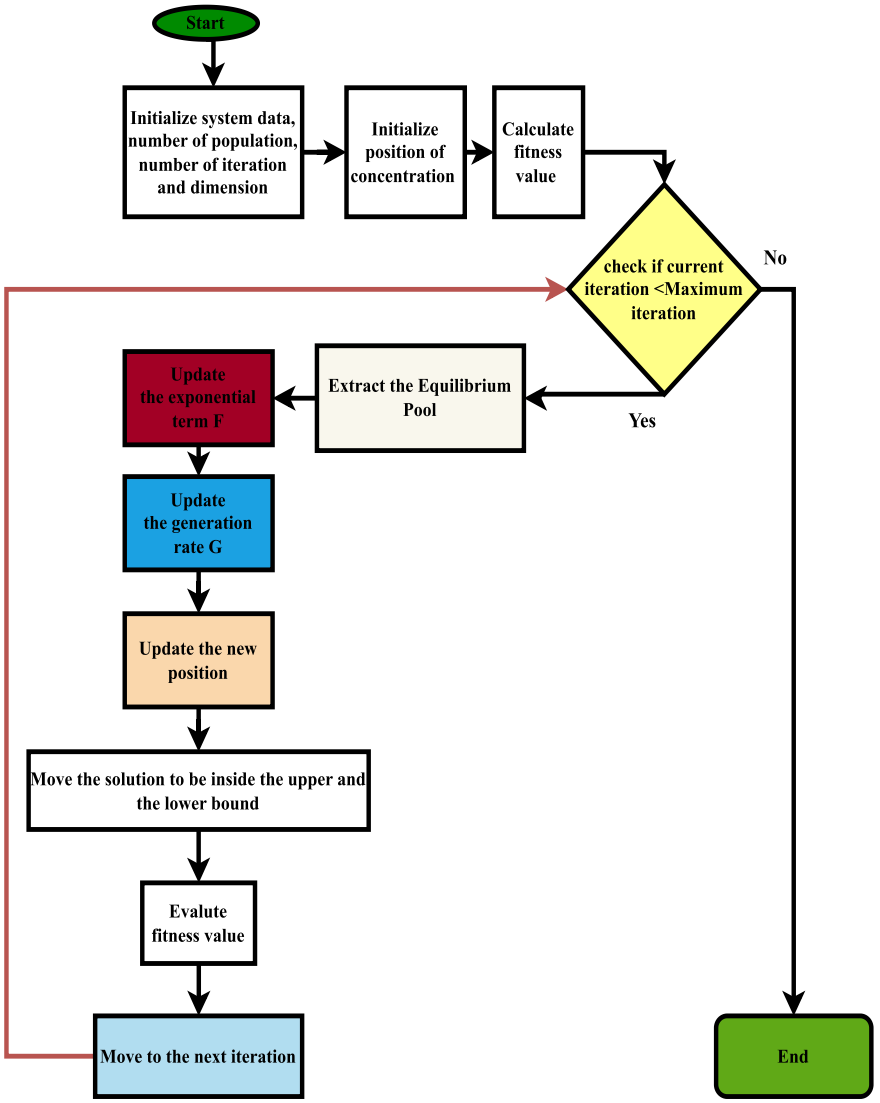

Fig. 6. The schematic diagram of the EO process.

3.2. Equilibrium Optimizer (EO)

EO is an algorithm based on mass equilibrium models used in various engineering fields, including physical applications founded on the conservation of mass principle. This principle is formulated through the equation of mass change rate being equivalent to the inflow rate minus the outflow rate coupled with the generated mass [60]. In the EO algorithm, particles strive to reach equilibrium, representing the optimal solution attainable within the exploration space. The solution's position can be expressed as the concentration. The equilibrium concentration, also known as the equilibrium pool, comprises one of the best solutions achieved by combining five other candidate solutions [61]. The schematic diagram of the EO process is depicted in Fig. 6.

3.3. The ESMO-based MPPT technique

The ESMO algorithm combines the two fundamental algorithms' best features, leveraging the EO's equilibrium pool feature to reduce stochasticity in the second equation. This integration enables the SMA to approach the best optimal solution more efficiently and rapidly [62]. The algorithmic outline of the ESMO approach is showcased in Algorithm 1.

Where t denotes the ongoing iteration, and $MaxIter$ designates the maximum iteration. U_b and L_b signify the upper and lower confines of the exploration space. At iteration, k, Y_A, and Y_B are designated as two random individuals drawn from the entire colony, and Z is equal to 0.03. r_1 and r_2 are random values between 0 and 1. υ_b is a uniform distribution within the range (-α, α), and υ_c is a uniform distribution within the range (-β, β), where α and β are equal to:

Algorithm 1: The pseudo-code of ESMO.

Input: N, D, $MaxIter$, Ub, Lb, z
Output: $Ygbest$
Initialization: Initialize $Y_i = \{y_i^1, y_i^2, \ldots, y_i^D\}$ for $i = 1, 2, \ldots, N$ at random positions within the search boundary $[Lb, Ub]$ using Eq. (8) for D dimensions at iteration $k = I$. Form $Y = \{\vec{Y}_1, \vec{Y}_2, \ldots, \vec{Y}_N\}$;
while $t \leq MaxIter$ **do**
  Evaluate the fitness $f(Y)$ of the N slime moulds;
  Sort the fitness values using Eq. (13) and determine $fitLbest$ and $fitLworst$;
  Construct the $Yeq.pool$ using Eq. (15);
  Determine the weighting factor W using Eq. (14);
  Update the global best position $Ygbest$;
  Determine a using Eq. (10) and b using Eq. (11);
  for $i = 1$ *to* N **do**
    Generate a random value r_1;
    if $r_1 < z$ **then**
      Update the position vector $\vec{Y}_i(t+1) = r_1 \cdot (Ub - Lb) + Lb$;
    else
      Update the probability p, vb, vc;
      Randomly choose one position vector Yeq from the equilibrium pool;
      Generate a random value r_2;
      if $r_2 < p$ **then**
        Select a random position vector $\vec{Y}_B$ from Y;
        Update the position vector $\vec{Y}_i(t+1) = \vec{Y}_{Gbest} + v_b \cdot (\vec{W} \cdot \vec{Y}_{cq} - \vec{Y}_B)$;
      else
        Update the position vector $\vec{Y}_i(t+1) = v_c \cdot \vec{Y}_i(t)$;
      end
    end
  end
  Increment $t = t + 1$;
end
return $Ygbest$

$$alpha = \arctan h(-(\frac{t}{MaxIter}) + 1) \tag{8}$$

and

$$beta = 1 - (\frac{t}{MaxIter}) \tag{9}$$

The value of p_i is presented in Equation (10).

$$p_i = \tanh\left|Z(i) - DF_{gbest}\right| \tag{10}$$

Where $Z(i)$ represents the fitness of $Y(i)$, and DF denotes the top fitness achieved throughout all iterations.

The weight factor in the current iteration is formulated by sorting the fitness values for a maximization problem. The weight W_g is given by Equation (11):

$$\begin{gathered}[sortfit, sortIndex] = sort(fit) \quad fit = \left\{fit_1, fit_2, ..., fit_N\right\} \\ Wg(sortIndex(j)) = \left\{\begin{array}{ll} 1 + r_3 \cdot \log(\frac{f_{best} - sortfit(j)}{f_{best} - f_{worst}} + 1) & 1 \leq j \leq \frac{N}{2} \\ 1 - r_3 \cdot \log(\frac{f_{best} - sortfit(j)}{f_{best} - f_{worst}} + 1) & \frac{N}{2} < j \leq N \end{array}\right\} \end{gathered} \tag{11}$$

Where r_3 is a random number spans from 0 to 1, and the best and worst fitness values are denoted by f_{best} and f_{worst}, which are equal to $sortfit(N)$ and $sortfit(1)$, respectively.

In the second equation of the Slime Mould Algorithm, the random terms Y_A and Y_B could be a factor in the slow and ineffective search process, leading to difficulties in recognizing the global solution in optimization problems. Although the paper [48] discussed positive results, there exists potential for additional enhancement in striving towards the optimal solution. Inspired by the EO, the equilibrium pool (C_{eq}) can be utilized to replace the random variable Y_A.

The slime mould individual of the equilibrium pool is presented as:

$$\begin{gathered} Y_{eq(1)} = Y(sortIndex(N)) \\ Y_{eq(2)} = Y(sortIndex(N-1)) \\ Y_{eq(3)} = Y(sortIndex(N-2)) \\ Y_{eq(4)} = Y(sortIndex(N-3)) \\ Y_{avrg} = \frac{Y_{eq(1)} + Y_{eq(2)} + Y_{eq(3)} + Y_{eq(4)}}{4} \\ Y_{eq} = \left\{Y_{eq(1)}, Y_{eq(2)}, Y_{eq(3)}, Y_{eq(4)}, Y_{avrg}\right\} \end{gathered} \tag{12}$$

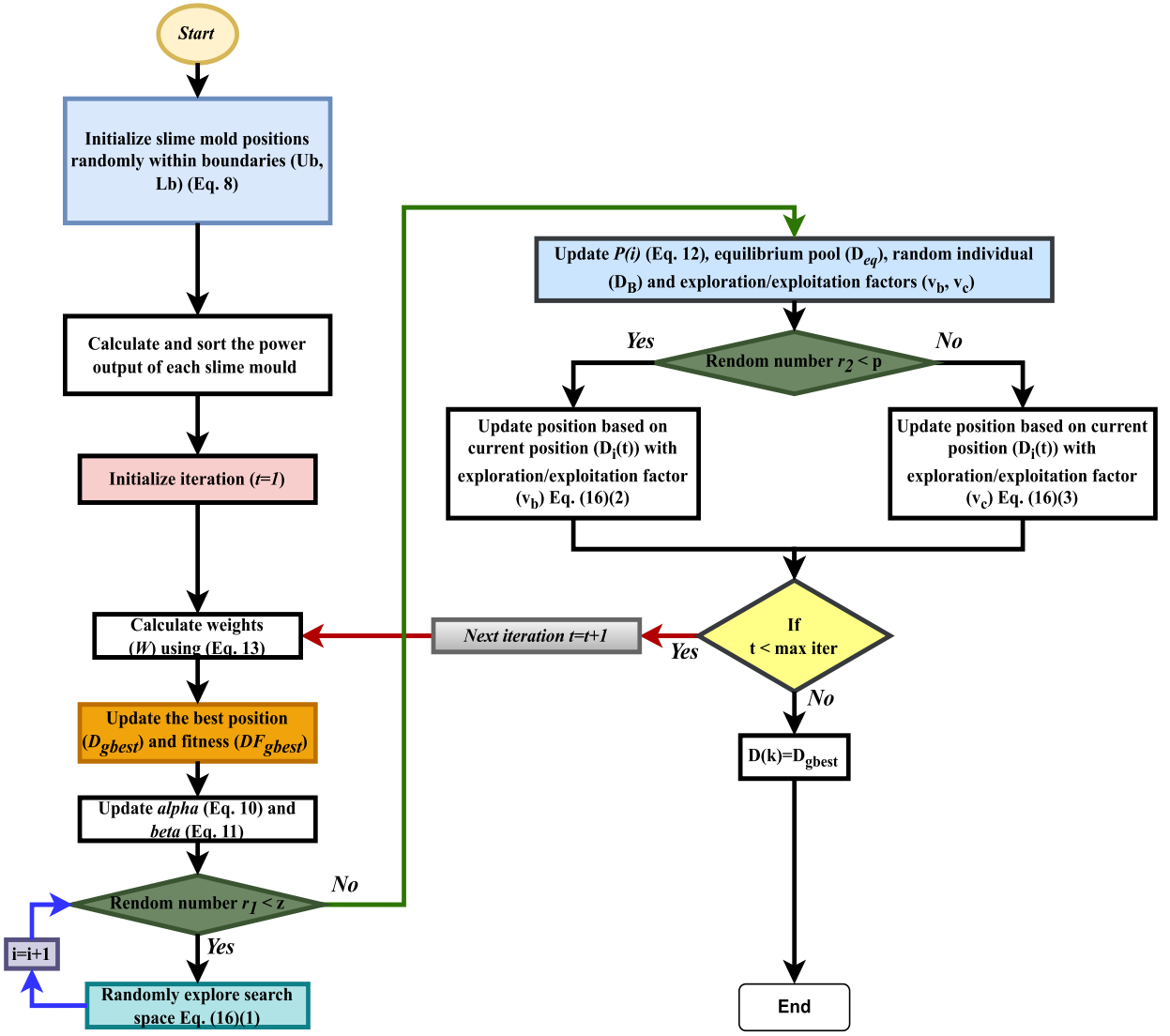

Fig. 7. The schematic depiction of the ESMO.

The new i_{th} slime mould position is now expressed using the new Equation (13):

$$Y_i(t+1) = \begin{cases} r_1 \cdot (Ub - Lb) + Lb, & , r_1 < z \\ Y_{Gbest} + v_b \cdot (W \cdot Y_{eq} - Y_B) & r_2 < p_i(t), r_1 \geq z \\ v_c \cdot Y_i(t) & r_2 \geq p_i(t), r_1 \geq z \end{cases} \tag{13}$$

Note that the new term helps strike a balance between the exploratory and exploitative phases, where the equilibrium pool array allows the process to gain great control during the search. The adjustment of the DCL is carried out following Equation (14).

$$D_i(t+1) = \begin{cases} r_1 \cdot (Ub - Lb) + Lb, & , r_1 < z \\ D_{Gbest} + v_b \cdot (W \cdot D_{eq} - D_B) & r_2 < p_i(t), r_1 \geq z \\ v_c \cdot D_i(t) & r_2 \geq p_i(t), r_1 \geq z \end{cases} \tag{14}$$

Here, $D(t+1)$ denotes the revised DCL, D_{Gbest} stands for the DCL of the global best, D_B represents a randomly selected DCL from the colony D_{eq} signifies a random DCL chosen from the Equilibrium pool consisting of the top five best DCLs achieved up to this point. The schematic depiction of the ESMO is displayed in Fig. 7.

Equation (15) represents the objective function employed by the proposed ESMO for converging toward the best DCL. This equation continuously compares the power generated by each individual ($P_i(t)$) with the previously identified global best power ($P_{Gbest}(t-1)$).

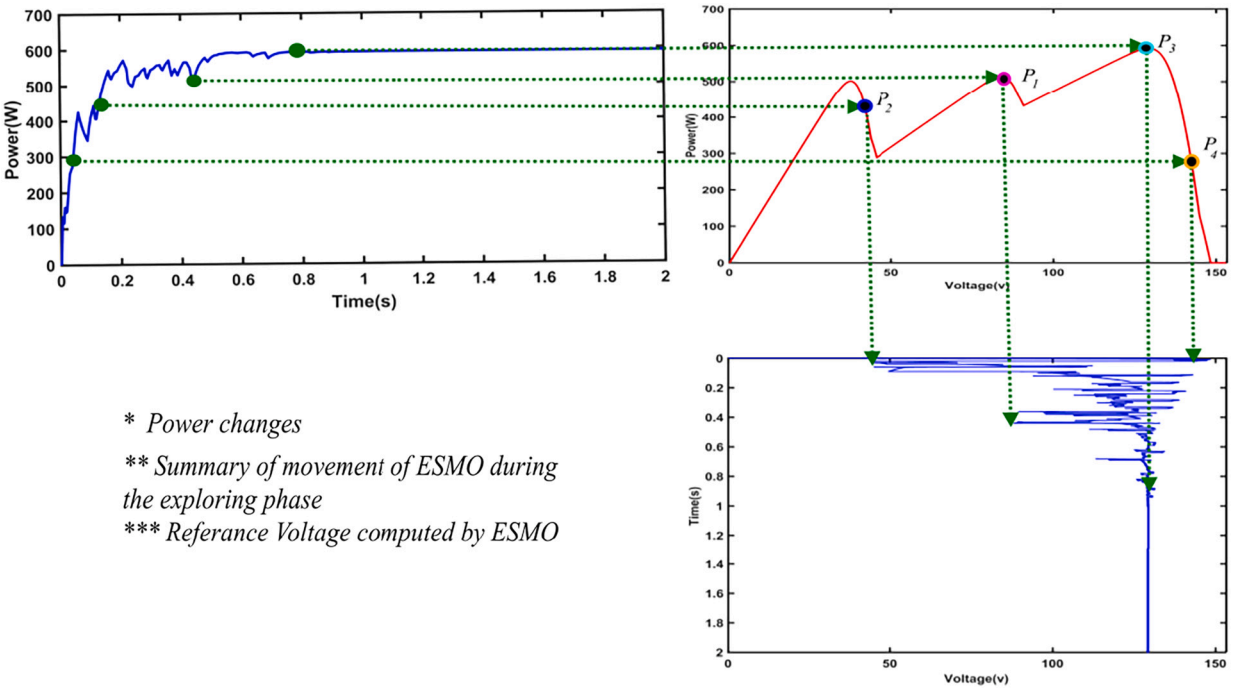

Fig. 8. The tracking mechanism of the ESMO-based MPPT.

$$\begin{aligned} &if \;\; P_i(t) > P_{Gbest}(t-1) \\ &\quad P_{Gbest}(t) = P_i(t) \\ &\quad D_{Gbest}(t) = D_i(t) \end{aligned} \tag{15}$$

If the value of $P_i(t)$ surpasses the previously recorded $P_{Gbest}(t-1)$, the objective function also updates the current $D_i(t)$ as $D_{Gbest}(t)$ which guarantees continuously maximizing power generation.

Equation (16) guarantees that the search will be repeated if there is a change in the value of the irradiation or the shading condition (DPSC), which leads to a new GMPP value so that if this condition exceeds 3%, it will be triggered. In addition, this ensures that the search will not be repeated during the change in the load value.

$$\frac{\left|P_{Gbest}(t) - P_{Gbest}(t-1)\right|}{P_{Gbest}(t-1)} > 0.03 \tag{16}$$

3.4. Tracking mechanism

The ESMO algorithm derives the reference voltage aligned to the MPP from the PV curve, which is considered a non-linear search space. Within 40 milliseconds, four particles are randomly initialized in the exploration space, and the process continues as a value between 0 and 1 expressed in the DCL. The PV curve contains one GMPP with a value of 592.1 W and two LMPP with a value of LM1 = 512 W and LM2 = 501 W. The ESMO algorithm continues to search for the GMPP until it is identified. The ESMO algorithm moves on to the exploitation stage after identifying the GMPP, and the particles approach each other concerning the best particle until they reach the best voltage value corresponding to the highest power point. Fig. 8 illustrates the ESMO-based MPPT tracking mechanism.

4. Results and discussion

The results were executed under the MATLAB/SIMULINK environment, with a simulation time step of 1e-5 s. The detailed implementation of the proposed ESMO-based MPPT technique is depicted in Fig. 9. The simulations were conducted using MATLAB R2016a version (The MathWorks, Inc., Natick, MA, USA).

The efficacy of the new ESMO technique was tested in three different cases:

- Case (1): FIC.
- Case (2): PSC.
- Case (3): CPSC.

The ESMO technique was compared to the two fundamental techniques, SMO and EO, and other well-known techniques like GWO, WOA, and the classical PSO.

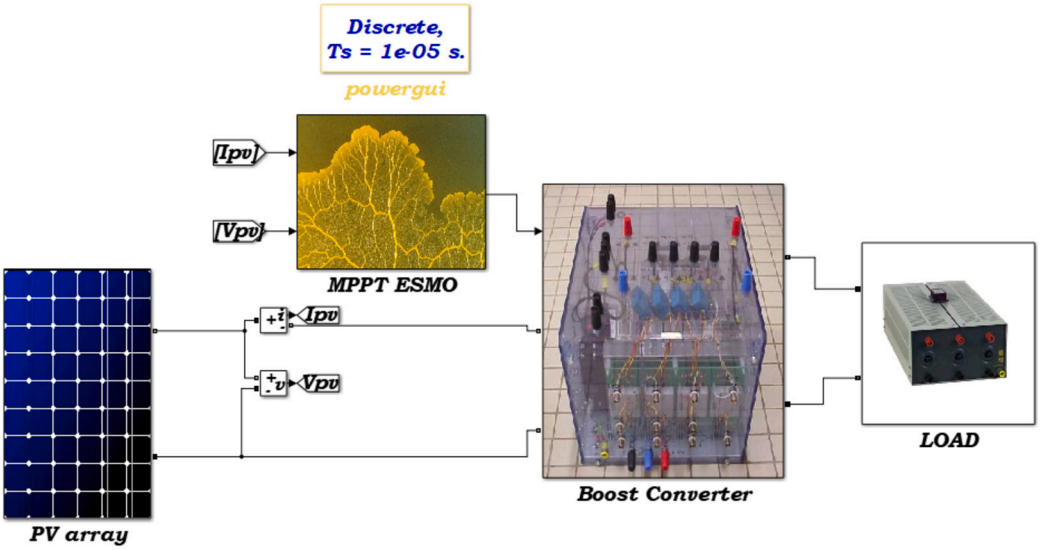

Fig. 9. ESMO-based MPPT Simulink Block.

Table 3
Irradiance pattern for PSC case 2.

Case No.	Irradiance (W/m^2)	GMPP(W)
Case 2 Partial Shading condition	PV1 = 310 PV2 = 190 PV3 = 510 PV4 = 440 PV5 = 120	321.8

4.1. Under FIC

The study was conducted under the scenario of fast changes in Irradiation. The modules received uniform values of Irradiation in successive time intervals. The results obtained were as follows: Fig. 10(a) shows the power response during the three fast Irradiation changes in the mentioned intervals. The ESMO technique achieved the lowest reaching time of 0.25 s and settling time of 0.4 s in the first interval, with a maximum power tracked at 157.8 W. In comparison, SMO, EO, GWO, WOA, and PSO achieved convergence times of 0.35 s, 0.4 s, 0.37 s, 0.3 s, and 0.4 s, settling times of 0.4 s, 0.5 s, 0.4 s, 0.32 s, and 0.6 s, and maximum power tracked of 157.75 W, 156 W, 157.35 W, 157.79 W, and 156.6 W, respectively. Fig. 10(b) illustrates the searching process of the DCL. In the second interval, the ESMO technique achieved a 0.1 s rapid convergence and stabilization duration of 0.12 s, with a maximum power tracked at 61.5 W. In contrast, SMO, EO, GWO, WOA, and PSO achieved convergence times of 0.22 s, 0.4 s, 0.2 s, 0.16 s, and 0.3 s, settling times of 0.25 s, 0.42 s, 0.21 s, 0.2 s, and 0.55 s, and maximum power tracked of 61.4 W, 60 W, 60.5 W, 61.48 W, and 60 W, respectively. The effectiveness of the ESMO technique was evident in these results. Similarly, in the third interval, the ESMO technique achieved the lowest reaching time of 0.205 s and settling time of 0.212 s, with a maximum power tracked at 110.06 W. In comparison, SMO, EO, GWO, WOA, and PSO achieved reaching times of 0.21 s, 0.213 s, 0.212 s, 0.206 s, and 0.21 s, settling times of 0.23 s, 0.22 s, 0.22 s, 0.209 s, and 0.215 s, and maximum power tracked of 109.7 W, 110 W, 110 W, 110 W, and 108.6 W, respectively. Fig. 10(c) and Fig. 10(d) illustrate the searching process for the optimal voltage and current, respectively.

4.2. Partial shading conditions (PSC)

PSC is studied using the 5SP1 configuration under the irradiance values shown in Table 3. The PV curve pattern obtained during PSC has a GMPP value of 321.8 W, shown in Fig. 11. The proposed ESMO technique successfully identified the GMPP with high efficiency, achieving the shortest adaptation period of 0.25 s, the shortest stabilization time of 0.28 s, and the highest power value estimated at 321.77 W with an impressive efficiency of 99.99% in only seven iterations. Fig. 12(a) presents the power response during the PSC, highlighting the superiority of ESMO over the other techniques, including SMO, EO, GWO, WOA, and PSO. These techniques obtained power values of 321.7 W, 321.7 W, 320 W, 321.5 W, and 318 W, with convergence times equal to 0.4 s, 0.41 s, 0.55 s, 0.45 s, and 1.1 s, and settling times equal to 0.45 s, 0.44 s, 0.62 s, 0.5 s, and 1.3 s, respectively, over several iterations ranging from 11 to 21. Fig. 12(b) represents the DCL of the techniques used in this work. The PV voltage and the PV current are illustrated in Fig. 12(c) and Fig. 12(d), respectively, showcasing the efficient tracking of the GMPP by the proposed ESMO technique in the presence of PSC.

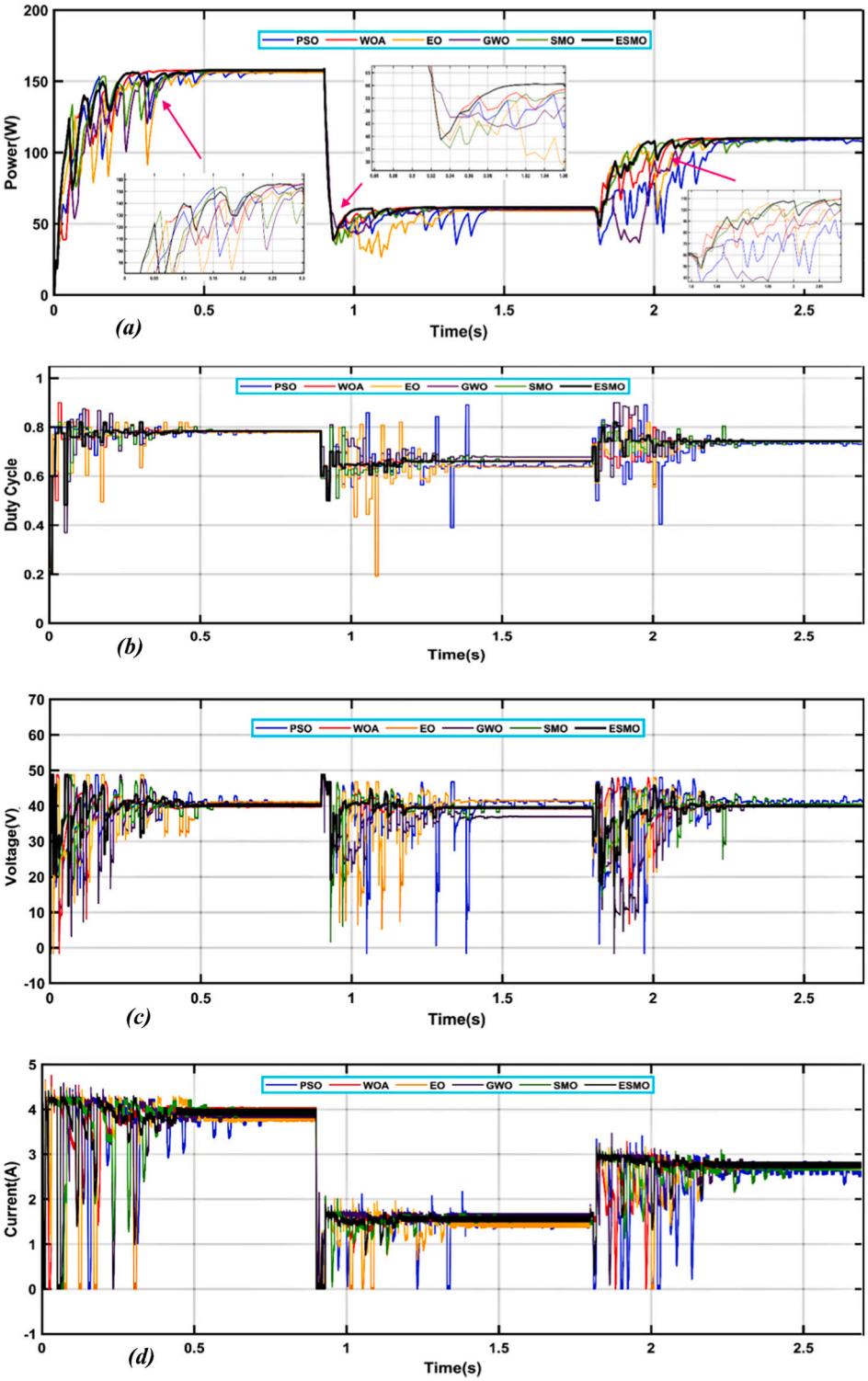

Fig. 10. Case 1 FIC: (a) Power output comparison of the techniques; (b) DCLs comparison of the techniques; (c) PV voltage comparison of the techniques; (d) PV current comparison of the techniques.

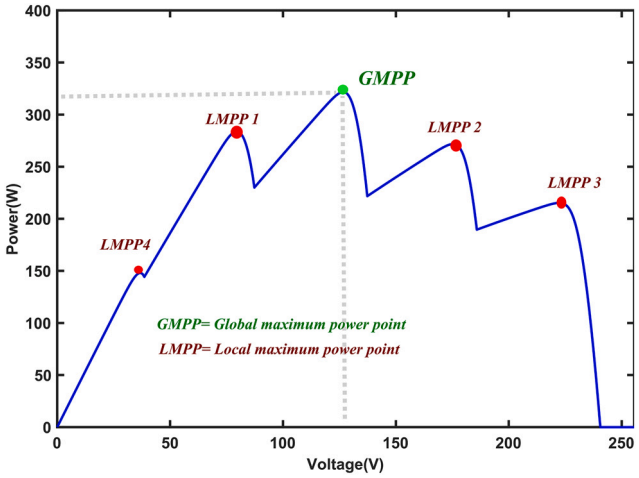

Fig. 11. PV curve pattern during PSC condition.

Table 4
Irradiance pattern for CPSC case 3.

Case No.	Irradiance (W/m^2)	GMPP(W)
Case 3 Complex Partial Shading conditions	PV1 = 300 PV2 = 60 PV3 = 505 PV4 = 345 PV5 = 905 PV6 = 225 PV7 = 435 PV8 = 315 PV9 = 660 PV10 = 830	873.83

4.3. CPSC

In many PV systems, multiple modules are utilized to produce a higher power output. However, in scenarios where shading occurs, a complex PSC state is formed. This results in the PV curve having several peaks and clusters. Fig. 13 illustrates the PV curve during the CPSC. To simulate the CPSC, specific irradiance values are applied, as shown in Table 4. Additionally, Fig. 13 portrays the PV curve during CPS condition with cluster formation.

In this case, the PV curve displays two discernible groupings, denoted as Cluster 1 and Cluster 2. Cluster 1 includes LM4 = 704 W, LM5 = 773.3 W, and LM6 = 754.6 W, while Cluster 2 consists of LM7 = 805.2, LM8 = 873.83 W, and LM9 = 849 W. The cluster head maxima (CHM) represents the MPP within each cluster, with CHM1 = LM5 and CHM2 = LM8. GMPP corresponds to the overall peak on the PV curve, and its value is GMPP = LM8 = 873.83 W. Fig. 14(a) presents the power response comparison among the techniques. The proposed ESMO technique outperformed the others, achieving the shortest response time of 0.21 s and reaching the time of 0.22 s, and required the fewest iterations (6) to identify the GMPP. On the other hand, SMO, EO, GWO, WOA, and PSO obtained convergence times of 0.32 s, 0.37 s, 0.37 s, 0.45 s, and 0.8 s, respectively, with reaching times of 0.4 s, 0.38 s, 0.38 s, 0.55 s, and 0.85 s, along with a higher number of iterations (ranging from 7 to 18). Fig. 14(b) presents the DCL comparison among the techniques. The hybridization of the two basic techniques in the proposed ESMO played a critical role during the exploratory and exploitative phases, enabling it to identify the GMPP even under CPSC efficiently. The PV voltage and current for the fourth case are illustrated in Fig. 14(c) and Fig. 14(d), respectively. Table 5 presents a comprehensive overview of all the examined scenarios.

4.4. Experimental validation

The proposed algorithm was thoroughly examined to validate its superiority. Initially, the ESMO algorithm's theoretical performance was assessed through MATLAB/Simulink simulations. Following this theoretical verification, the ESMO algorithm efficiency was experimentally evaluated within a laboratory setup. Fig. 15 shows the experimental setup of the PV system. The experimental system schema, including the MATLAB blocks and the controlling principal of the PV emulator, is presented in Fig. 16, and The electrical parameters are shown in Table 6.

To accurately emulate the output of the PV array under PSC and DPSC, a programmable power supply, specifically the GWINSTEK-APS1102A, was employed. This power supply facilitated precise simulation, mimicking the behavior of the PV array. It was crucial to experimentally verify the output of the programmable power supply to ensure its conformity with the PV array's output. Fig. 17 demonstrates the P-V/I-V curve pattern employed for this verification, and Fig. 18 shows the output of the power supply on specific points on the I-V curve. The accuracy of the power supply can be observed through its ability to accurately emulate the behavior of the PV array, specifically in replicating the non-linear characteristics of the cell's equation. This was achieved by measuring multiple random points along the I-V curve and confirming that the power supply's output aligns with the expected measurement.

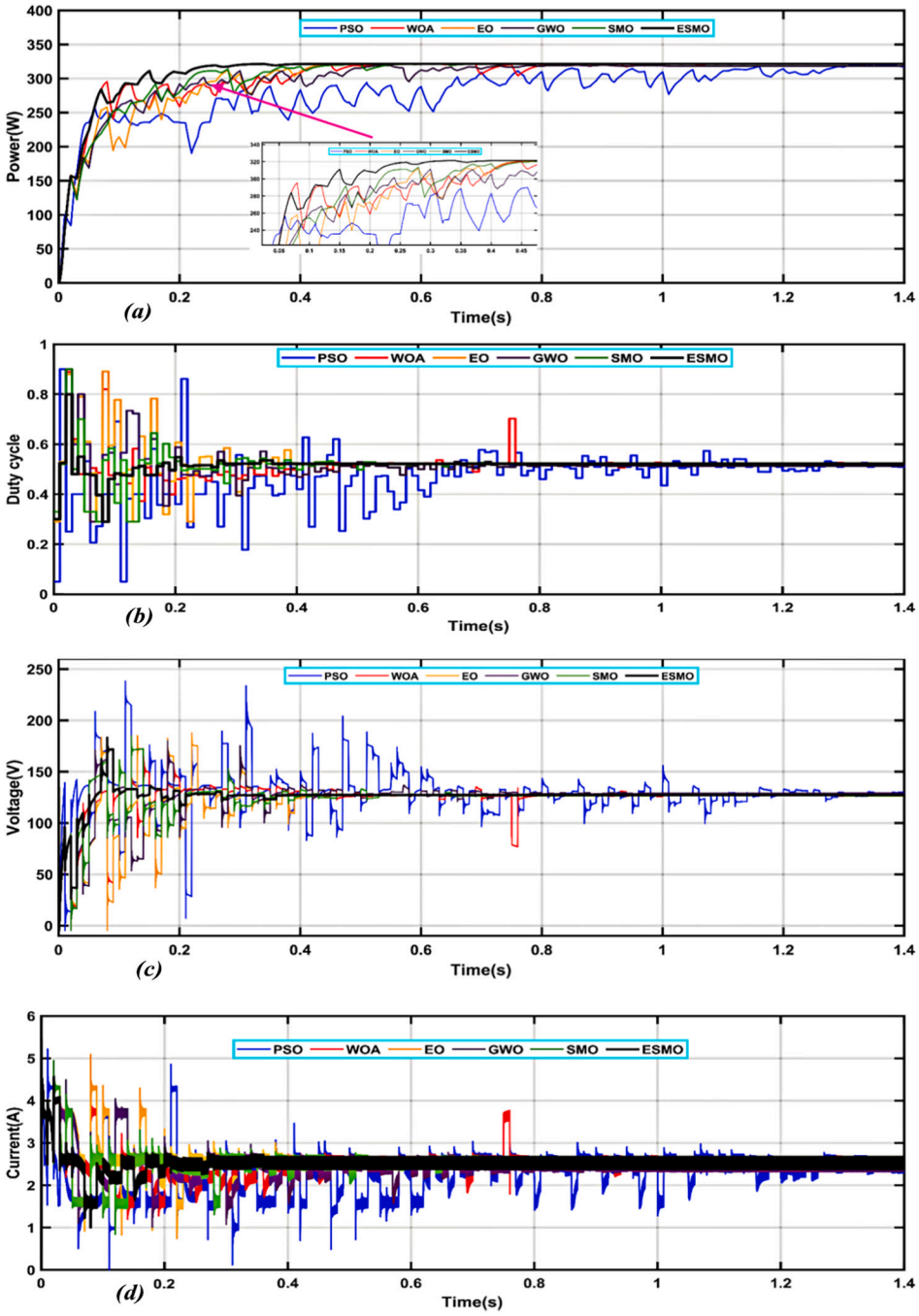

Fig. 12. Case 2 PSC: (a) Power output comparison of the techniques; (b) DCLs comparison of the techniques; (c) pv voltage comparison of the techniques; (d) pv current comparison of the techniques.

Furthermore, the PV array emulator was controlled by the DCL of the DC-DC boost converter, which was effectively connected to the dSPACE1104 R&D Controller Board. A sampling frequency of 20 kHz was adopted to maintain accurate control over the input. The DCL Update Timer (DCUT) was set to 40 Hz, equivalent to 25 ms. This particular time interval was determined to facilitate the transition of DCL values from one state to another within the control algorithm. This value was selected based on careful observation and analysis of the algorithm's control state as executed by the DSpace board. The objective behind this choice was to achieve a steady state condition that ensures the code execution does not overrun or result in divergent behavior. By carefully tuning the DCUT to 40 Hz, the system effectively maintains stability and enhances the overall performance of the control process.

In the context of comparable simulation experiments, the proposed algorithm ESMO was empirically validated, demonstrating its superiority in two distinct P-V curve scenarios of the PV system: PSC and DPSC. These two curves, as depicted in Fig. 19, were

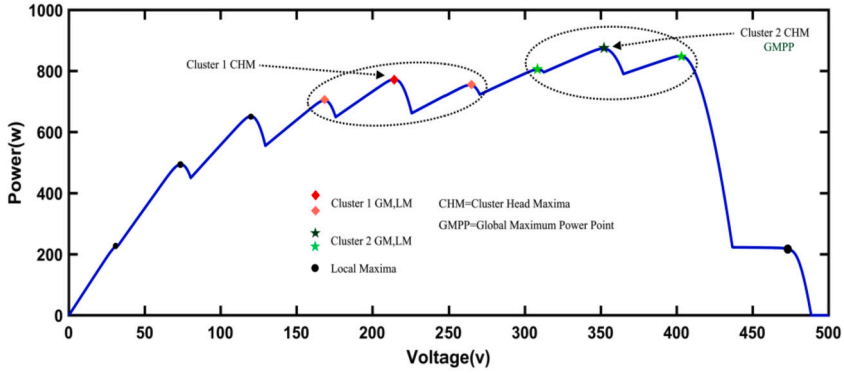

Fig. 13. PV curve during CPS condition with cluster formation.

Table 5
In-depth comparison of all the studied cases.

Tech.	Case no.	Converge time (s)	Settling time (s)	GMPP (W)	Power tracked (W)	Iteration Number	Avg Efficiency (%)
ESMO	Case 1	0.25, 0.1, 0.205	0.4, 0.12, 0.212	157.8, 61.5, 110.06	157.8, 61.5, 110.06	10	99.99
	Case 2	0.25	0.28	321.8	321.77	7	99.99
	Case 3	0.21	0.22	873.83	873.5	6	99.96
SMO	Case 1	0.35, 0.22, 0.21	0.4, 0.25, 0.23	157.8, 61.5, 110.06	157.75, 61.4, 109.7	18	99.82
	Case 2	0.4	0.45	321.8	321.7	13	99.96
	Case 3	0.32	0.4	873.83	870.1	8	99.57
EO	Case 1	0.4, 0.4, 0.213	0.5, 0.42, 0.22	157.8, 61.5, 110.06	156, 60, 110	15	98.78
	Case 2	0.41	0.44	321.8	321.7	12	99.96
	Case 3	0.37	0.38	873.83	871.2	9	99.69
GWO	Case 1	0.37, 0.2, 0.212	0.4, 0.21, 0.22	157.8, 61.5, 110.06	157.35, 60.5, 110	18	99.34
	Case 2	0.55	0.62	321.8	320	15	99.44
	Case 3	0.37	0.38	873.83	869	7	99.44
WOA	Case 1	0.3, 0.16, 0.206	0.32, 0.2, 0.209	157.8, 61.5, 110.06	157.79, 61.48, 110	13	99.96
	Case 2	0.45	0.5	321.8	321.5	11	99.90
	Case 3	0.45	0.55	873.83	865	12	98.98
PSO	Case 1	0.4, 0.3, 0.21	0.6, 0.55, 0.215	157.8, 61.5, 110.06	156.6, 60, 108.6	20	98.48
	Case 2	1.1	1.3	321.8	318	21	98.81
	Case 3	0.8	0.85	873.83	858.28	18	98.22

Table 6
The electrical parameters of the experimental setup.

Description	Values
Inductance (L)	30 mH
capacitance (C)	1100 uF
Load Resistance (R_L)	30 Ω
Switching freq (f)	20 kHz
Duty Cycle Update Timer ($DCUT$)	40 Hz

employed, featuring two different global values of maximum power, namely 269 W, and 236 W, along with two corresponding maximum voltage values of 60.4 V and 60.8 V, and two maximum current values of 4.45 A and 3.85 A, respectively. In the first case, all algorithms successfully identified the global maximum value. However, the proposed algorithm ESMO exhibited a distinct advantage over others in terms of reaching speed and reaching time, as depicted by the red line in Fig. 20. Notably, ESMO achieved the fastest reaching time, recording an estimated time of 200 ms. In comparison, other algorithms, SMO, EO, GWO, WOA, and PSO, demonstrated longer reaching times, registering values of 350 ms, 425 ms, 575 ms, 350 ms, and 775 ms, respectively. The results highlight ESMO's superior performance, confirming its effectiveness in swiftly converging toward the GMPP.

In the second case, involving DPSC, the algorithms' capacity to re-identify the new maximum value estimated at 236 W was effectively evaluated following a modification in the external perimeter of the PV system. The experimental results of the second case are shown in Fig. 21. In this context, the proposed algorithm demonstrated the swiftest response time, estimated at 200 ms, showcasing its efficient and rapid adaptability. Conversely, other algorithms, namely SMO, EO, GWO, WOA, and PSO, exhibited longer response times, recording values of 325 ms, 500 ms, 450 ms, 400 ms, and 950 ms, respectively. The results unequivocally validate the proposed

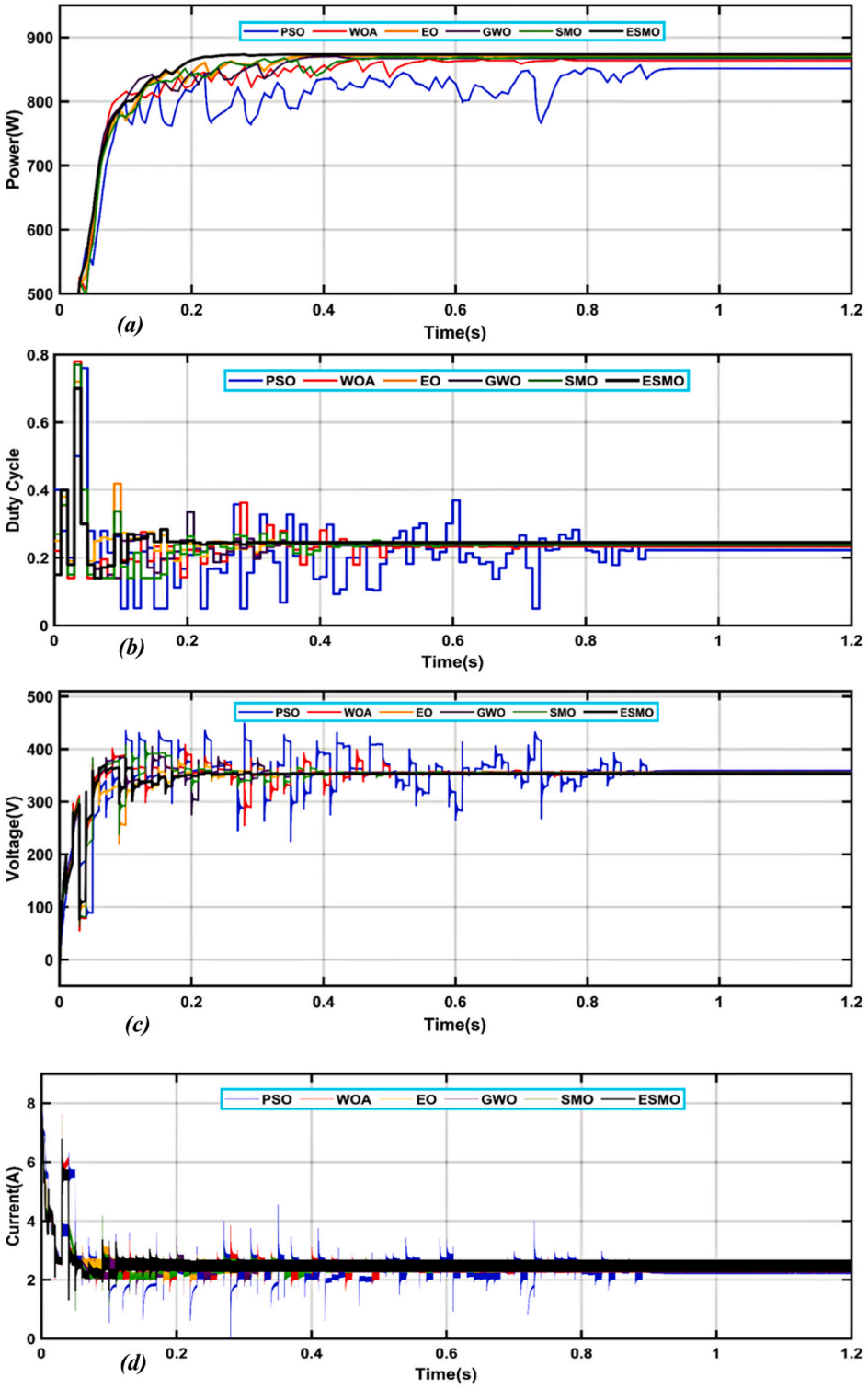

Fig. 14. Case 3 CPSC: (a) Power output comparison of the techniques; (b) DCLs comparison of the techniques; (c) pv voltage comparison of the techniques; (d) pv current comparison of the techniques.

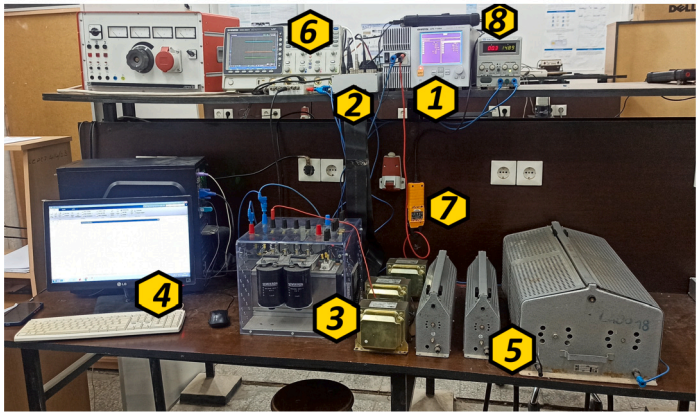

Fig. 15. Image of the experimental setup (1—PV emulator, 2—dSPACE 1104, 3—DC-DC converter, 4—The Host computer, 5—resistor load, 6—oscilloscope, 7—current sensors, 8—voltage sensors).

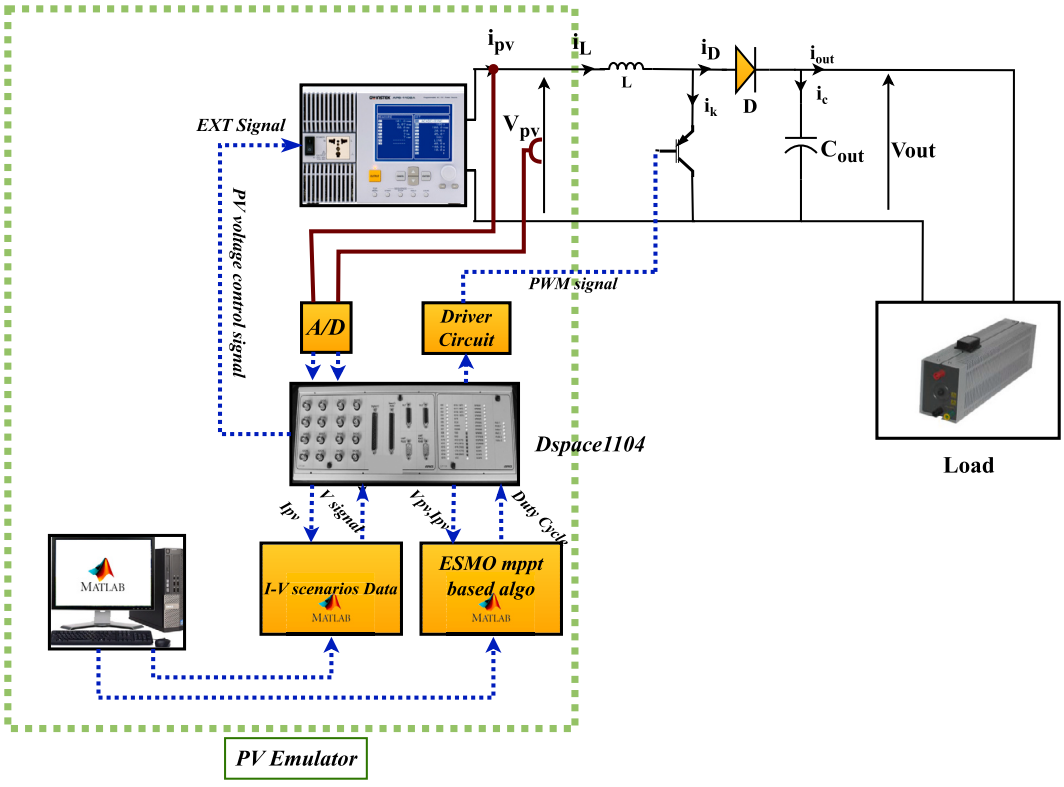

Fig. 16. Experimental schema block for proposed ESMO-based MPPT.

Table 7
Comparison of experimental results.

Tech.		ESMO	SMO	EO	GWO	WOA	PSO
Response time (ms)	PSC	200	350	425	575	350	775
	DPC	200	325	500	450	400	950

algorithm's superior performance in swiftly adjusting to the dynamic changes in the system, ensuring quicker convergence towards the new maximum value of 236 W under these varying conditions. Table 7 presents a comparison of experimental results.

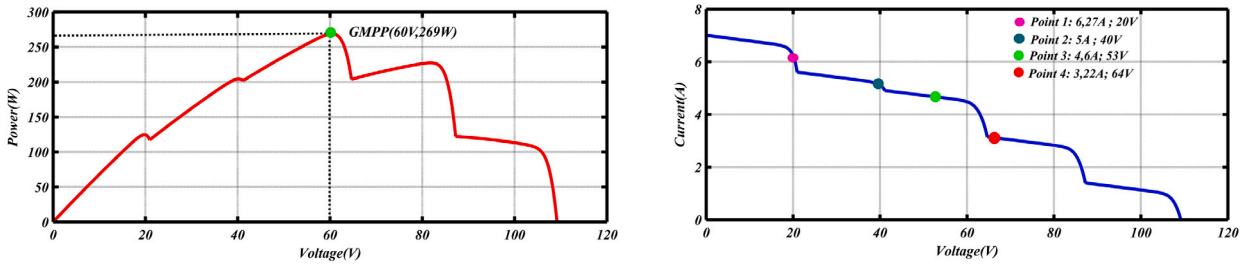

(a) P-V curve (b) I-V curve

Fig. 17. P-V and I-V curve of the verification.

(a) Point 1 (b) Point 2

(c) Point 3 (d) Point 4

Fig. 18. The output of the power supply on specific points on the I-V curve.

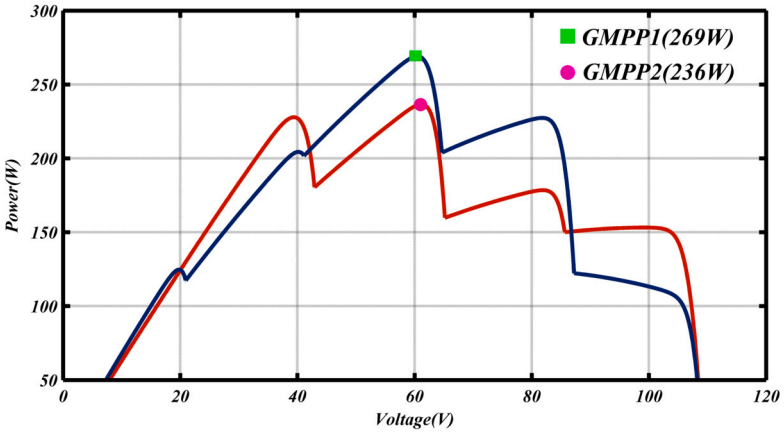

Fig. 19. The two P-V curve pattern of case 1 and case 2.

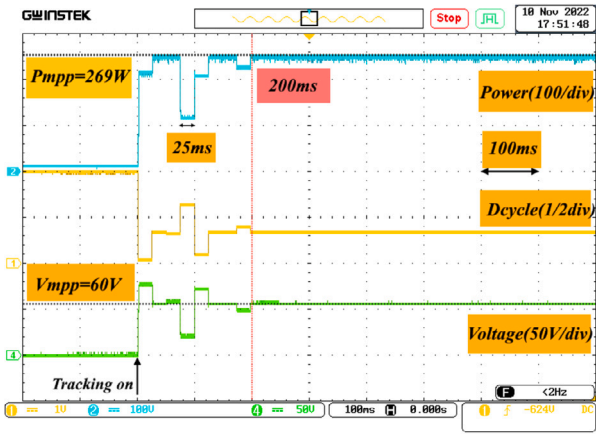

(a) The proposed ESMO

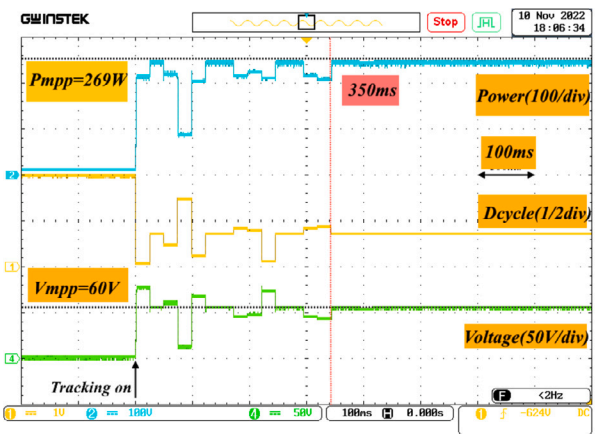

(b) SMO

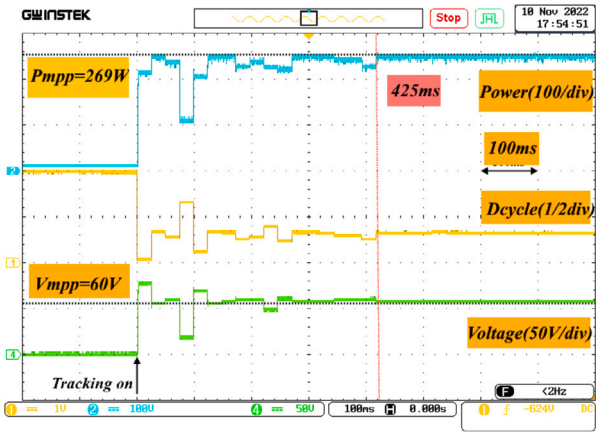

(c) EO

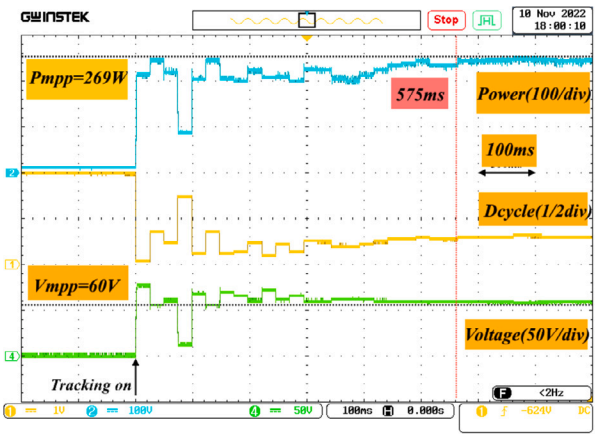

(d) GWO

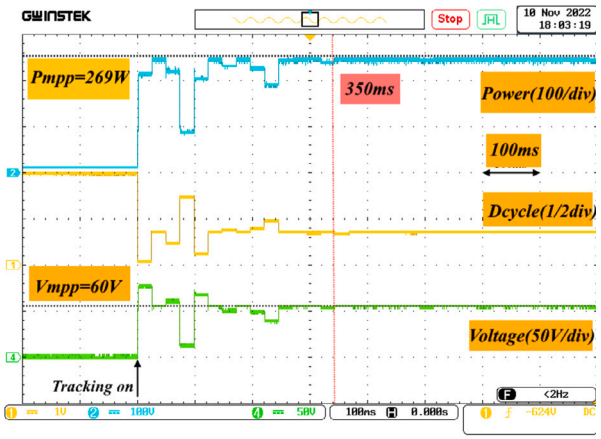

(e) WOA

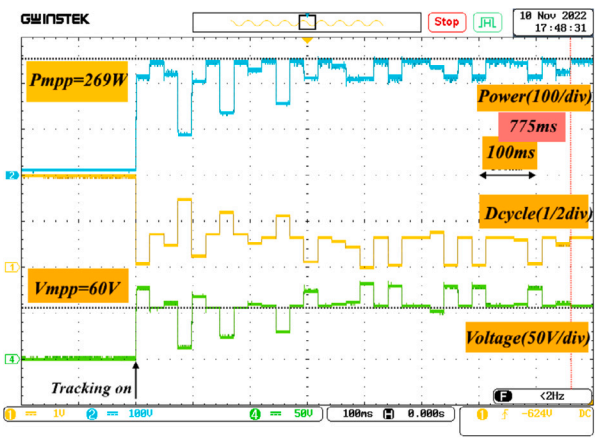

(f) PSO

Fig. 20. Case 1 PSC: The experimental results of the MPPT for (a) ESMO, (b) SMO, (c) EO, (d) GWO, (e) WOA, and (f) PSO.

5. Conclusions and perspectives

The research paper introduces a novel Equilibrium ESMO technique for tracking the MPP in solar systems. ESMO combines two new techniques and models them as mathematical equations to serve as an MPPT-based control approach. The proposed technique is extensively tested in three distinct scenarios of PV systems, including FIC, PSC, and CPSC. Comparisons are made between ESMO and other MPPT techniques, namely Slime Mould Optimization (SMO), EO, Grey Wolf Optimization (GWO), Whale Optimization

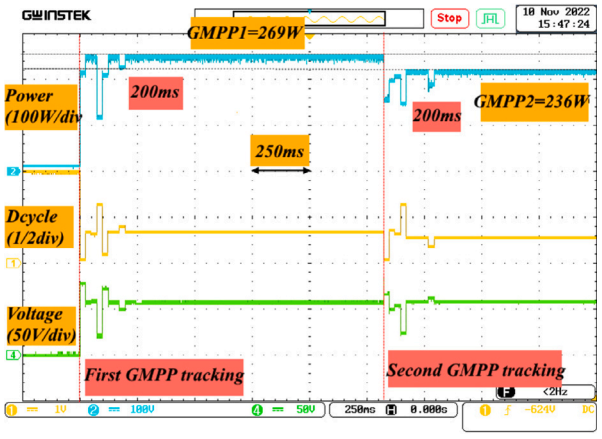

(a) The proposed ESMO

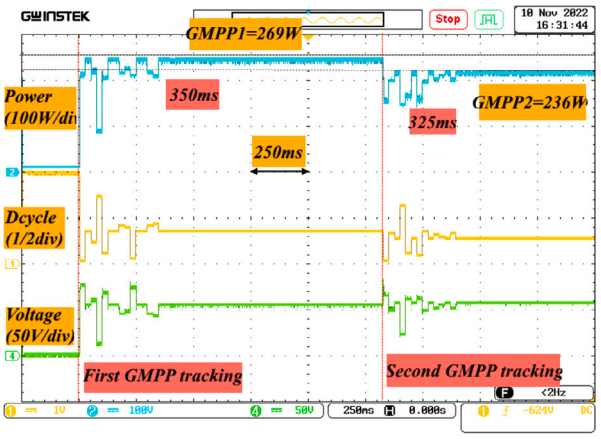

(b) SMO

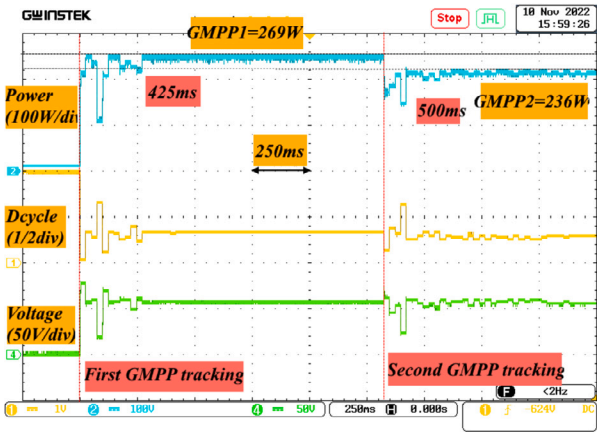

(c) EO

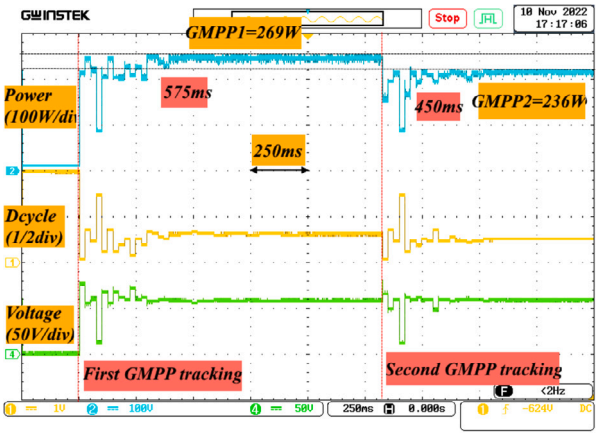

(d) GWO

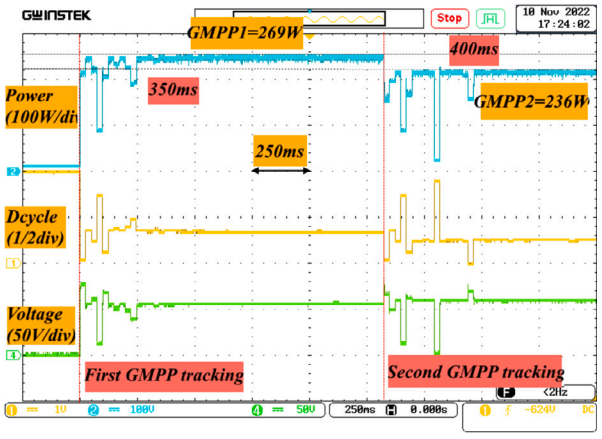

(e) WOA

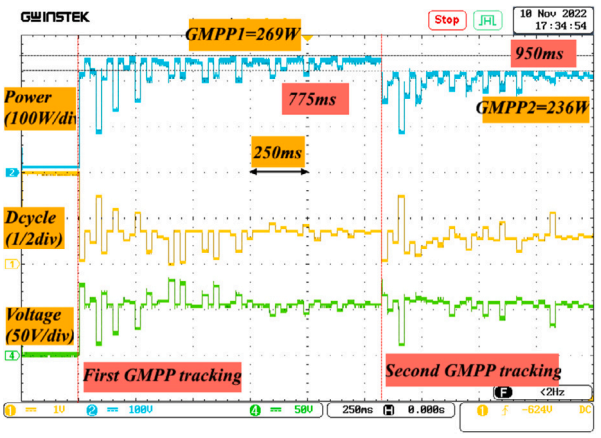

(f) PSO

Fig. 21. Case 2 DPSC: The experimental results of the MPPT for (a) ESMO, (b) SMO, (c) EO, (d) GWO, (e) WOA, and (f) PSO.

Algorithm (WOA), and PSO. The ESMO technique exhibits increased output power efficiency and reduced power losses in all cases. Simulation using MATLAB/SIMULINK and a comparative statistical study underscore the efficacy and robustness of ESMO, with an impressive average efficiency of up to 99.98 percent in all scenarios, including CPSC, where some techniques struggle with local maxima trapping. Moreover, the proposed algorithm's strength is further verified through experimental testing in two PV system cases, PSC and Dynamic Partial shading conditions (DPSC). ESMO recorded the fastest response times, identifying the two GMPPs within 200 ms. These experimental results affirm ESMO's effectiveness in efficiently handling varying conditions of PV systems. It is

noteworthy that ESMO effectively addresses the slow convergence observed in the SMO algorithm by incorporating the equilibrium pool feature of EO. This unique combination enhances the rapid adaptability and performance of ESMO under challenging conditions. Despite the proposed ESMO algorithm's success in obtaining high-efficiency rates for tracking GMPP during the majority of irradiation scenarios, applying the proposed algorithm under large-scale scenarios requires more studies and considerations regarding data storage, computational resources, and implementation complexity. Since huge irradiation and temperature data will certainly be captured, searching for solutions to store and process this data is essential. The computational requirements of the algorithm could potentially limit its ability to identify the GMPP accurately under rapidly changing irradiation patterns. Future research will investigate optimization strategies to reduce the computational complexity of the ESMO algorithm while maintaining its effectiveness in PSC. Additionally, exploring hardware acceleration techniques could be beneficial for real-world deployments, especially in large-scale PV systems encountering PSC.

CRediT authorship contribution statement

Djallal Eddine Zabia: Writing – original draft, Software, Formal analysis, Data curation, Conceptualization. **Hamza Afghoul:** Writing – original draft, Software, Methodology, Formal analysis, Data curation. **Okba Kraa:** Writing – original draft, Methodology, Investigation, Formal analysis, Data curation, Conceptualization. **Yassine Himeur:** Writing – review & editing, Visualization, Supervision, Resources, Project administration, Funding acquisition. **Haitham S. Ramadan:** Writing – review & editing, Visualization, Supervision, Project administration, Formal analysis. **Istemihan Genc:** Writing – review & editing, Visualization, Supervision, Project administration, Investigation. **Abdoulkader I. Idriss:** Writing – review & editing, Supervision, Project administration, Investigation. **Sami Miniaoui:** Writing – review & editing, Visualization, Supervision, Investigation, Funding acquisition, Formal analysis. **Shadi Atalla:** Writing – review & editing, Visualization, Validation, Supervision, Resources, Project administration. **Wathiq Mansoor:** Writing – review & editing, Visualization, Supervision, Resources, Project administration, Funding acquisition.

Declaration of competing interest

The authors declare that they have no known competing financial interests or personal relationships that could have appeared to influence the work reported in this paper.

Acknowledgements

We want to acknowledge the LEPCI laboratory and Professor Fateh Krim for providing the experimental setup that was instrumental in completing the experimental results presented in this paper, facilitating our reception, and providing the laboratory's services.

Data availability statement

The data that support the findings of this study are available upon reasonable request.

References

[1] Y. Himeur, M. Elnour, F. Fadli, N. Meskin, I. Petri, Y. Rezgui, F. Bensaali, A. Amira, Next-generation energy systems for sustainable smart cities: roles of transfer learning, Sustain. Cities Soc. (2022) 104059.
[2] H. Abidi, L. Sidhom, I. Chihi, Systematic literature review and benchmarking for photovoltaic mppt techniques, Energies 16 (8) (2023), https://doi.org/10.3390/en16083509.
[3] H. Bousbiat, R. Bousselidj, Y. Himeur, A. Amira, F. Bensaali, F. Fadli, W. Mansoor, W. Elmenreich, Crossing roads of federated learning and smart grids: overview, challenges, and perspectives, arXiv preprint, arXiv:2304.08602, 2023.
[4] M.A. Husain, A. Tariq, S. Hameed, M.S.B. Arif, A. Jain, Comparative assessment of maximum power point tracking procedures for photovoltaic systems, Green Energy Environ. 2 (1) (2017) 5–17, https://doi.org/10.1016/j.gee.2016.11.001.
[5] V. Jaiswal, A. Wadehra, S. Bhalla, K.P.S. Rana, V. Kumar, Comment on "deep reinforcement learning approach for mppt control of partially shaded pv systems in smart grids", Appl. Soft Comput. 146 (2023), https://doi.org/10.1016/j.asoc.2023.110577.
[6] B. Aljafari, D. S, B. C, P.K. Balachandran, T.S. Babu, Power enhanced solar pv array configuration based on calcudoku puzzle pattern for partial shaded pv system, Heliyon 9 (5) (2023) e16041, https://doi.org/10.1016/j.heliyon.2023.e16041.
[7] C. Ben Regaya, H. Hamdi, F. Farhani, A. Marai, A. Zaafouri, A. Chaari, Real-time implementation of a novel mppt control based on the improved pso algorithm using an adaptive factor selection strategy for photovoltaic systems, ISA Trans. 146 (2024) 496–510, https://doi.org/10.1016/j.isatra.2023.12.024.
[8] Sameera, M. Tariq, M. Rihan, M. Ayan, A comprehensive review on the application of recently introduced optimization techniques obtaining maximum power in the solar pv system, Renew. Energy Focus 49 (2024), https://doi.org/10.1016/j.ref.2024.100564.
[9] T. Chen, A. Harrison, N.H. Alombah, M. Aurangzeb, S. Iqbal, H.A. Mahmoud, A simplified control algorithm for efficient and robust tracking of the maximum power point in pv systems, Control Eng. Pract. 148 (2024), https://doi.org/10.1016/j.conengprac.2024.105945.
[10] S. Ganesan, P.W. David, P.K. Balachandran, I. Colak, Power enhancement in pv arrays under partial shaded conditions with different array configuration, Heliyon 10 (2) (2024) e23992, https://doi.org/10.1016/j.heliyon.2024.e23992.
[11] Z. Alaas, G.e.A. Eltayeb, M. Al-Dhaifallah, M. Latifi, A new mppt design using pv-bes system using modified sparrow search algorithm based anfis under partially shaded conditions, Neural Comput. Appl. 35 (19) (2023) 14109–14128, https://doi.org/10.1007/s00521-023-08453-9.
[12] Z.B. Hadj Salah, S. Krim, M.A. Hajjaji, B.M. Alshammari, K. Alqunun, A. Alzamil, T. Guesmi, A new efficient cuckoo search mppt algorithm based on a super-twisting sliding mode controller for partially shaded standalone photovoltaic system, Sustainability 15 (12) (2023), https://doi.org/10.3390/su15129753.
[13] A. Harrison, N.H. Alombah, J. de Dieu Nguimfack Ndongmo, Solar irradiance estimation and optimum power region localization in pv energy systems under partial shaded condition, Heliyon 9 (8) (2023) e18434, https://doi.org/10.1016/j.heliyon.2023.e18434.

[14] N. Mendhe, A. Vidyarthi, An effective hybrid approach based control for the mppt of pv system under partial shading condition for indoor energy harvesting in smart homes, Multimed. Tools Appl. (2023), https://doi.org/10.1007/s11042-023-15069-7.
[15] P. Kumari, N. Kumar, B.K. Panigrahi, Rayleigh distribution based novel and efficient mppt algorithm for rooftop pv system with competence to distinguish different dynamics, IEEE Trans. Consum. Electron. 70 (1) (2024) 58–67, https://doi.org/10.1109/tce.2023.3296115.
[16] S. Sankarananth, P. Sivaraman, Performance enhancement of multi-port bidirectional dc-dc converter using resilient backpropagation neural network method, Sustain. Comput., Inform. Syst. 36 (2022), https://doi.org/10.1016/j.suscom.2022.100783.
[17] I.N. Mwine, H. Han, H. Liu, H. Wang, X. Zheng, L. Fei, A novel neural network based mppt method under partial shading conditions, https://doi.org/10.1109/PandaFPE57779.2023.10141350, 2023.
[18] S. Chtita, A. Derouich, S. Motahhir, A. El Ghzizal, A new mppt design using arithmetic optimization algorithm for pv energy storage systems operating under partial shading conditions, Energy Convers. Manag. 289 (2023), https://doi.org/10.1016/j.enconman.2023.117197.
[19] N. Deghfel, A.E. Badoud, F. Merahi, M. Bajaj, I. Zaitsev, A new intelligently optimized model reference adaptive controller using ga and woa-based mppt techniques for photovoltaic systems, Sci. Rep. 14 (1) (2024) 6827, https://doi.org/10.1038/s41598-024-57610-0.
[20] M. Paramasivam, S. Subramaniam, Emperor penguin optimization based mppt for pv system under different irradiation condition, Electr. Power Compon. Syst. 51 (15) (2023) 1546–1561, https://doi.org/10.1080/15325008.2023.2199756.
[21] S. Mirjalili, A. Lewis, The whale optimization algorithm, Adv. Eng. Softw. 95 (2016) 51–67, https://doi.org/10.1016/j.advengsoft.2016.01.008.
[22] P.K. Bonthagorla, S. Mikkili, Hardware implementation of a novel hybrid mppt technique for fast tracking of gmpp in solar pv system under pscs, Circuit World (2023), https://doi.org/10.1108/cw-06-2022-0183.
[23] S. Li, H. Chen, M. Wang, A.A. Heidari, S. Mirjalili, Slime mould algorithm: a new method for stochastic optimization, Future Gener. Comput. Syst. 111 (2020) 300–323, https://doi.org/10.1016/j.future.2020.03.055.
[24] A. Faramarzi, M. Heidarinejad, B. Stephens, S. Mirjalili, Equilibrium optimizer: a novel optimization algorithm, Knowl.-Based Syst. 191 (2020), https://doi.org/10.1016/j.knosys.2019.105190.
[25] J.-K. Shiau, Y.-C. Wei, B.-C. Chen, A study on the fuzzy-logic-based solar power mppt algorithms using different fuzzy input variables, Algorithms 8 (2) (2015) 100–127, https://doi.org/10.3390/a8020100.
[26] M.A. Husain, S.B. Pingale, A. Bakar Khan, A. Faiz Minai, Y. Pandey, R. Shyam Dwivedi, Performance analysis of the global maximum power point tracking based on spider monkey optimization for pv system, Renew. Energy Focus 47 (2023), https://doi.org/10.1016/j.ref.2023.100503.
[27] B. Aljafari, P.K. Balachandran, D. Samithas, S.B. Thanikanti, Solar photovoltaic converter controller using opposition-based reinforcement learning with butterfly optimization algorithm under partial shading conditions, Environ. Sci. Pollut. Res. Int. 30 (28) (2023) 72617–72640, https://doi.org/10.1007/s11356-023-27261-1.
[28] G.A. Ghazi, E.A. Al-Ammar, H.M. Hasanien, W. Ko, S.M. Lee, R.A. Turky, M. Tostado-Véliz, F. Jurado, Circle search algorithm-based super twisting sliding mode control for mppt of different commercial pv modules, IEEE Access 12 (2024) 33109–33128, https://doi.org/10.1109/access.2024.3372412.
[29] K. Xia, Y. Li, B. Zhu, Improved photovoltaic mppt algorithm based on ant colony optimization and fuzzy logic under conditions of partial shading, IEEE Access 12 (2024) 44817–44825, https://doi.org/10.1109/access.2024.3381345.
[30] C. Yuan, J. Xia, F. Huang, P. Zhao, L. Kong, A novel Hermite interpolation-based mppt technique for photovoltaic systems under partial shading conditions, IEEE Photonics J. 16 (2) (2024) 1–10, https://doi.org/10.1109/jphot.2024.3369869.
[31] P. Qi, H. Xia, X. Cai, M. Yu, N. Jiang, Y. Dai, Novel global mppt technique based on hybrid cuckoo search and artificial bee colony under partial-shading conditions, Electronics 13 (7) (2024), https://doi.org/10.3390/electronics13071337.
[32] B. Kumar, A. Kumar, A novel adaptive flower pollination algorithm for maximum power tracking of photovoltaic systems under dynamic shading conditions, Iran. J. Sci. Technol. Trans. Electr. Eng. (2024), https://doi.org/10.1007/s40998-024-00696-z.
[33] G.-R. Yu, Y.-D. Chang, W.-S. Lee, Maximum power point tracking of photovoltaic generation system using improved quantum-behavior particle swarm optimization, Biomimetics 9 (4) (2024), https://doi.org/10.3390/biomimetics9040223.
[34] G.A. Ghazi, E.A. Al-Ammar, H.M. Hasanien, W. Ko, J. Park, D. Kim, Z. Ullah, Dandelion optimizer-based reinforcement learning techniques for mppt of grid-connected photovoltaic systems, IEEE Access 12 (2024) 42932–42948, https://doi.org/10.1109/access.2024.3378749.
[35] H.L.D. Ha, L. Gopal, C.W.R. Chiong, F.H. Juwono, K.H. Law, A novel artificial location selection optimization for global maximum power point tracking under partial shading conditions, Energy Convers. Manag. 304 (2024), https://doi.org/10.1016/j.enconman.2024.118218.
[36] A.T. Naser, K.K. Mohammed, N.F.A. Aziz, K.b. Kamil, S. Mekhilef, Improved coot optimizer algorithm-based mppt for pv systems under complex partial shading conditions and load variation, Energy Convers. Manag., X 22 (2024), https://doi.org/10.1016/j.ecmx.2024.100565.
[37] K.-H. Chao, T.T.T. Bau, Global maximum power point tracking of photovoltaic module arrays based on an improved intelligent bat algorithm, Electronics 13 (7) (2024), https://doi.org/10.3390/electronics13071207.
[38] K.-H. Chao, T.B.-N. Nguyen, Global maximum power point tracking of a photovoltaic module array based on modified cat swarm optimization, Appl. Sci. 14 (7) (2024), https://doi.org/10.3390/app14072853.
[39] J. Katebi, M. Shoaei-parchin, M. Shariati, N.T. Trung, M. Khorami, Developed comparative analysis of metaheuristic optimization algorithms for optimal active control of structures, Eng. Comput. 36 (4) (2019) 1539–1558, https://doi.org/10.1007/s00366-019-00780-7.
[40] R. Thota, N. Sinha, A novel hybrid arithmetic-based grey wolf optimization method for tracking the global maximum power point of photovoltaic systems under unequal irradiance patterns, Arab. J. Sci. Eng. (2023), https://doi.org/10.1007/s13369-023-08006-1.
[41] M.A. Husain, A. Tariq, Transient analysis and selection of perturbation parameters for pv-mppt implementation, Int. J. Ambient Energy 41 (10) (2018) 1176–1182, https://doi.org/10.1080/01430750.2018.1517661.
[42] M. Naseem, M.A. Husain, A.F. Minai, A.N. Khan, M. Amir, J. Dinesh Kumar, A. Iqbal, Assessment of meta-heuristic and classical methods for gmppt of pv system, Trans. Electr. Electron. Mater. 22 (3) (2021) 217–234, https://doi.org/10.1007/s42341-021-00306-3.
[43] Y. Li, L. Li, Y. Jiang, Y. Gan, J. Zhang, S. Yuan, A novel hybrid maximum power point tracking technique for pv system under complex partial shading conditions in campus microgrid, Appl. Sci. 13 (8) (2023), https://doi.org/10.3390/app13084998.
[44] Z.-K. Fan, K.-L. Lian, J.-F. Lin, A new golden eagle optimization with stooping behaviour for photovoltaic maximum power tracking under partial shading, Energies 16 (15) (2023), https://doi.org/10.3390/en16155712.
[45] U. Yadav, A. Gupta, R. kr Ahuja, Hardware validation of hybrid MPPT technique via Novel ML controller and P&O method, Energy Rep. 8 (2022) 77–84.
[46] H.S. Ramadan, A.F. Bendary, S. Nagy, Particle swarm optimization algorithm for capacitor allocation problem in distribution systems with wind turbine generators, Int. J. Electr. Power Energy Syst. 84 (2017) 143–152, https://doi.org/10.1016/j.ijepes.2016.04.041.
[47] A. Ballaji, R. Dash, V. Subburaj, J.R. Kalvakurthi, D. Swain, S.C. Swain, Design & development of mppt using pso with predefined search space based on fuzzy Fokker Planck solution, IEEE Access 10 (2022) 80764–80783, https://doi.org/10.1109/access.2022.3195036.
[48] A.F. Mirza, M. Mansoor, K. Zhan, Q. Ling, High-efficiency swarm intelligent maximum power point tracking control techniques for varying temperature and irradiance, Energy 228 (2021), https://doi.org/10.1016/j.energy.2021.120602.
[49] J.V.G. Rama Rao, S. Venkateshwarlu, S.A. Saleem, S. Arandhakar, S. Ruttala, Optimizing solar panel maximum power point tracking and parasitic parameter extraction in partial shading with enhanced slime mold optimization, Meas., Sens. 33 (2024), https://doi.org/10.1016/j.measen.2024.101163.
[50] K. Buch, H.R. Chavan, Current Sensorless PO-PSO MPPT Control for PV Systems Based on Dynamic Observer, 2023, pp. 1–6.
[51] A. Atoui, M. Kermadi, M. Seghir Boucherit, K. Benmansour, S. Barkat, F. Akel, S. Mekhilef, A fast and accurate global maximum power point tracking controller for photovoltaic systems under complex partial shadings, Int. J. Electr. Comput. Eng. 13 (1) (2023), https://doi.org/10.11591/ijece.v13i1.pp69-84.

[52] S.K. Vankadara, S. Chatterjee, P.K. Balachandran, An accurate analytical modeling of solar photovoltaic system considering rs and rsh under partial shaded condition, Int. J. Syst. Assur. Eng. Manag. 13 (5) (2022) 2472–2481, https://doi.org/10.1007/s13198-022-01658-6.
[53] S. Suman, D. Chatterjee, R. Mohanty, Power quality improvement for microgrid-connected pv-based converters under partial shading conditions using mixed optimisation algorithms, Int. J. Bio-Inspir. Comput. 21 (3) (2023) 123–136, https://doi.org/10.1504/ijbic.2023.131918.
[54] M. Dhimish, A.M. Tyrrell, Power loss and hotspot analysis for photovoltaic modules affected by potential induced degradation, npj Mater. Degrad. 6 (1) (2022), https://doi.org/10.1038/s41529-022-00221-9.
[55] N. Douifi, A. Abbadi, F. Hamidia, K. Yahya, M. Mohamed, N. Rai, A novel mppt based reptile search algorithm for photovoltaic system under various conditions, Appl. Sci. 13 (8) (2023), https://doi.org/10.3390/app13084866.
[56] P.K. Bonthagorla, S. Mikkili, A novel hybrid slime mould mppt technique for bl-hc configured solar pv system under pscs, J. Control Autom. Electr. Syst. 34 (4) (2023) 782–795, https://doi.org/10.1007/s40313-023-00996-5.
[57] A.O. Salau, G.K. Alitasb, Mppt efficiency enhancement of a grid connected solar pv system using finite control set model predictive controller, Heliyon 10 (6) (2024) e27663, https://doi.org/10.1016/j.heliyon.2024.e27663.
[58] E. Özkalay, F. Valoti, M. Caccivio, A. Virtuani, G. Friesen, C. Ballif, The effect of partial shading on the reliability of photovoltaic modules in the built-environment, EPJ Photovolt. 15 (2024), https://doi.org/10.1051/epjpv/2024001.
[59] H. Gundogdu, A. Demirci, S.M. Tercan, U. Cali, A novel improved grey wolf algorithm based global maximum power point tracker method considering partial shading, IEEE Access 12 (2024) 6148–6159, https://doi.org/10.1109/access.2024.3350269.
[60] H. Rehman, I. Sajid, A. Sarwar, M. Tariq, F.I. Bakhsh, S. Ahmad, H.A. Mahmoud, A. Aziz, Driving training-based optimization (dtbo) for global maximum power point tracking for a photovoltaic system under partial shading condition, IET Renew. Power Gener. 17 (10) (2023) 2542–2562, https://doi.org/10.1049/rpg2.12768.
[61] H. Rezk, M. Aly, A. Fathy, A novel strategy based on recent equilibrium optimizer to enhance the performance of pem fuel cell system through optimized fuzzy logic mppt, Energy 234 (2021), https://doi.org/10.1016/j.energy.2021.121267.
[62] M.K. Naik, R. Panda, A. Abraham, An entropy minimization based multilevel colour thresholding technique for analysis of breast thermograms using equilibrium slime mould algorithm, Appl. Soft Comput. 113 (2021), https://doi.org/10.1016/j.asoc.2021.107955.